The role of SPEF2 in spermatogenesis

Suvi Virtanen

Pro gradu –tutkielma

Turun yliopisto
Biologian laitos
24.9.2016

Linja: fysiologian ja genetiikan linja
Erikoistumislinja: fysiologia

Laajuus: 40 op

Tarkastaja:

1:

2:

Hyväksytty (pvm):

Arvolause:

University of Turku
Department of Biology
Faculty of Natural Sciences

VIRTANEN, SUVI: The role of SPEF2 in spermatogenesis

Master's thesis 51 p.
Physiology
May 2016

Correct sperm head shaping and tail assembly are important for male fertility. A deleterious mutation in *Sperm flagellar protein 2* (*Spef2*) gene (also known as *Kpl2*) has been implicated to disrupt the sperm tail formation in Finnish Yorkshire pigs and big giant head (bgh) mice. SPEF2 has been postulated to have a role in intraflagellar transport (IFT) and has been shown to interact with IFT20, an IFT complex B protein. In this study, a novel conditional male germ cell specific knock-out mouse model (Spef2 cKO) was used to study the role of SPEF2 in spermatogenesis. The aim of the study was to characterize the phenotype of the Spef2 cKO mouse model and test the functionality of novel anti-SPEF2 antibodies. The phenotyping was carried out with histological and immunofluorescent stainings. Novel anti-SPEF2 antibodies were evaluated with immunofluorescence and western blot methods. In addition to defective tail formation, the loss of functional SPEF2 seems to cause defective manchette clearance resulting in club-shaped sperm heads. Therefore, SPEF2 may participate in intramanchette transport (IMT). In addition, Spef2 cKO mice were shown to express multiple gamma-tubulin-positive signals from the basal bodies indicating a possible basal body -defect. An anti-SPEF2 antibody against the KAD domain appeared to function on western blot and drying down samples where it was shown to localize in the basal body and midpiece of sperm tail during the late spermiogenesis.

KEY WORDS: Spef2, male fertility, spermatogenesis, spermiogenesis, manchette, IMT, IFT

Contents

1 Introduction

1.1 Male fertility

According to the estimation by Boivin et al. (2007) one in seven couples (around 80 million people) is affected by infertility problems worldwide. It is estimated that in 25-28% cases the cause of infertility is idiopathic i.e. the cause remains unknown (Hull et al. 1985, Brandes et al. 2010, Brandes et al. 2011, NICE 2013). Male infertility alone accounts for around 30% of all reported infertility cases (NICE 2013). Most common defined reason for infertility is sperm dysfunction (Hull et al. 1985, Irvine 1998). Currently there is no non-assisted reproduction treatment to enhance the sperm quality available mainly because the underlying knowledge of molecular and cellular biology affecting the sperm is insufficient (Barratt et al. 2011).

In addition to human fertility problems, improved knowledge on animal fertility is also needed. In food production reproduction efficiency of high-producing dairy and beef cattle has declined for decades (Sheldon & Dobson 2003, Beever 2006) . Low pregnancy rates and persistently high embryonic mortality create significant losses for the breeders (Moore & Thatcher 2006). According to industry estimates of reproductive efficiency for cattle, sheep, and swine, males seem to play an essential role in fertility problems (Flowers 2013). Deteriorated semen quality caused by inbreeding has also affected other species of economic interest, such as dog breeds (Wildt et al. 1982), and many endangered species, such as Puerto Rican parrots (*Amazona vittata*) (Clubb et al. 2015). Thus, additional knowledge on factors affecting the sperm quality could greatly benefit the breeding programs of domesticated animals and conservation efforts of endangered species.

1.2 Spermatogenesis

A process where diploid spermatogonial stem cells evolve into haploid male germ cells (spermatozoa) is called spermatogenesis (Figure 1). It takes place in the seminiferous tubules of the testis. Mammalian spermatogenesis starts when diploid spermatogonia undergo several mitotic divisions that give rise to spermatocytes. Spermatocytes then undergo two meiotic divisions to produce haploid spermatids. In the last phase of spermatogenesis (spermiogenesis) haploid spermatids start to differentiate into mature spermatozoa. This differentiation process includes the formation of an acrosome, assembly and elongation of the sperm tail, elimination of the excess cytoplasm, condensation of nuclear chromatin and reorganization of the organelles (Hermo et al. 2010a).

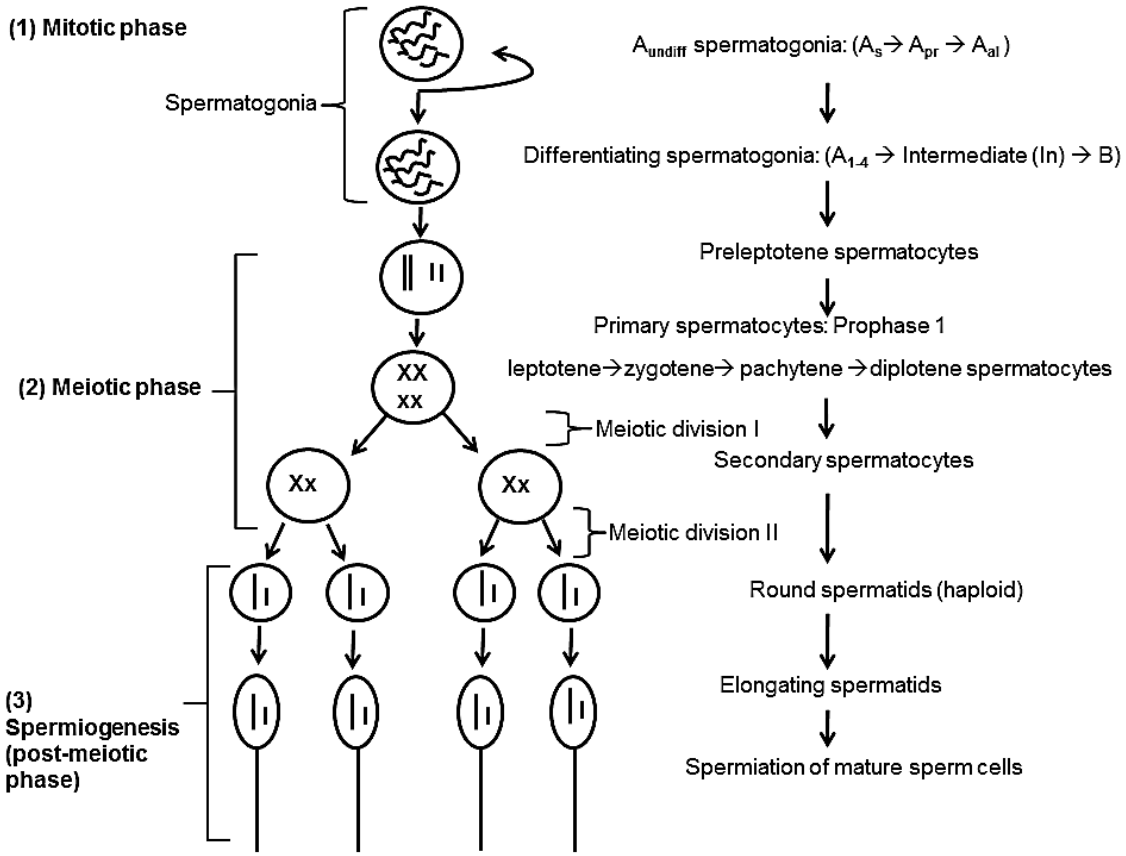

Figure 1. Schematic representation of spermatogenesis. During spermatogenesis the diploid spermatogonia evolve into haploid mature sperm cells via three distinctive phases: proliferation of spermatogonial stem cells and spermatogonia (mitotic phase), meiotic divisions of spermatocytes into haploid spermatids (meiotic phase) and differentiation of spermatids into mature sperm cells (post-meiotic phase, spermiogenesis). The A_{undiff} spermatogonia include spermatogonial stem cell population. They engage in self-renewal and produce the progeny for the following steps of spermatogenesis. The differentiating spermatogonia give rise to the preleptotene spermatocytes from which the primary spermatocytes are born. The majority of meiotic phase is spent in the prophase I during which the rearrangement of genetic material occurs. Spermiogenesis includes the elongation of spermatids and tail assembly. It ends with the spermiation of mature sperm cells into the lumen of seminiferous tubule.

1.2.1 The first phase of spermatogenesis: spermatogonia

The continuity of spermatogenesis relies on spermatogonial stem cells (Hermo et al. 2010a). Spermatogonial stem cells are constantly replenishing their numbers while providing a new set of germ cells for each cycle of spermatogenesis (Hermo et al. 2010a). According to the classical single isolated type A spermatogonium –model (A_s-model) by Huckins et al. (1971a, 1971b, 1971c) spermatogonia in mice can be divided into four categories: A_s spermatogonia, mitotic and undifferentiated spermatogonia (paired A spermatogonia, A_{pr} and aligned spermatogonia, A_{al}), differentiating spermatogonia (A_1-A_4, Intermediate (In) and B spermatogonia). The differentiating spermatogonia differ in morphology and in gene expression from the A_{undiff} cells (Hermo et al. 2010a, Yoshida 2012). Differentiating spermatogonia have more condensed

heterochromatin, bigger nucleus sizes and more cell organelles (Hermo et al. 2010a). Within the A_{undiff} the different cell populations can also be distinguished by gene expression profile (Yoshida 2012). A_s spermatogonium give rise to the A_{pr} spermatogonium population. A_{pr} as a result of uncompleted cell division of A_s are connected by intercellular bridges (Yoshida 2012). The presence of intercellular bridges among A_{pr} and their progeny is a sign of commitment to differentiate (Hermo et al. 2010a). The A_{al} -cell compartment is born from synchronized proliferation of A_{pr} cells (Hermo et al. 2010a). The first class of differentiating A_1 spermatogonia is born from the A_{al} compartment (Sugimoto et al. 2012). A_1 spermatogonia undergo four subsequent cell divisions (A_2, A_3, A_4, In) to produce B spermatogonia (Yoshida 2008).

1.2.2 The second phase of spermatogenesis: spermatocytes

The second phase of spermatogenesis consists of DNA replication and two subsequent meiotic divisions (Figure 1). Spermatocytes with diploid chromosome number before meiosis I are termed as primary spermatocytes, whereas the spermatocytes after meiosis I with diploid chromosome number are termed as secondary spermatocytes (Hermo et al. 2010a). Haploid spermatids are formed after the second meiotic division. A rearrangement of genetic material between homologous chromosomes (homologs) takes place during the first meiotic division. In mammals the prophase of meiosis I is the most time consuming part of the second phase of spermatogenesis (Hermo et al. 2010a). Prophase I is divided into five substages that include leptonema, zygonema, pachynema, diplonema and diakinesis (Cohen et al. 2006). Each substage has a correspondent spermatocyte: leptotene, zygotene, pachytene and diplotene spermatocyte, respectively (Figure 1).

B spermatogonia give rise to preleptotene (Pl) spermatocytes that move through the blood testis barrier (BTB) created by Sertoli cells from the basal compartment to the adluminal compartment of seminiferous epithelium (Yoshida 2008). Preleptotene spermatocytes begin DNA synthesis and chromosome replication which give rise to the tetraploid leptotene spermatocytes (O'Donnell & O'Bryan 2014). Leptotene spermatocytes initiate the condensation of chromatin structure and the alignment of homologs (Cohen et al. 2006). After the alignment of homologs is completed in zygotene spermatocytes the formation of synapsis (pairing of homologs) is initiated (Cohen et al. 2006). Formation of chiasma structure between non-sister chromatids is a physical manifestation of crossing-over (Hermo et al. 2010a). Crossing-over occurs when non-sister chromatids exchange corresponding chromatid segments (Hermo et al. 2010a). During the longest substage of prophase I, pachynema, homologous recombination is completed (O'Donnell & O'Bryan 2014). Desypnasis takes place in

diplotene spermatocytes and is followed by diakinesis, shortening of chromosomes (Hermo et al. 2010a). During metaphase I homologous chromosomes are aligned and connected to meiotic spindle apparatus which pulls them to the opposite side of cell during anaphase I (O'Donnell & O'Bryan 2014). The first meiotic division is completed during the telophase and consequent division of cytoplasm results in secondary spermatocytes (Hermo et al. 2010a). Secondary spermatocytes with haploid number of chromosomes and diploid DNA content enter meiosis II and give rise to haploid round spermatids (Hermo et al. 2010a).

1.2.3 The last phase of spermatogenesis: elongation of spermatids

Spermiogenesis starts with the emergence of round spermatids and ends with the spermiation, a process where spermatids are detached from Sertoli cells and are released into the lumen of seminiferous tubules. Differentiation of spermatids includes assembly and the elongation process of sperm tail, shaping of the sperm head, acrosome biogenesis, formation of the transient manchette, condensation of nuclear chromatin and the removal of excess cytoplasm into residual bodies (Hermo et al. 2010a). During the condensation chromatin histones are first replaced with transition proteins and then with protamines (Borg et al. 2010). Most mammals have only one type of protamine while mice and humans have two types: protamine 1 (PRM1) and protamine 2 (PRM2) (Borg et al. 2010).

1.2.4 Cycle of seminiferous epithelium

Germ cells in different phases of development together with Sertoli cells form the seminiferous epithelium (Hess & de Franca 2008). Synchronized changes in the cell content of epithelium occur in repetitious cycles (Hess & de Franca 2008, Ahmed & de Rooij 2009). The cycle of seminiferous epithelium can be divided into specific stages based on the different cell content found within the epithelium (Hess & de Franca 2008). The number of the stages depends on the species (Hermo et al. 2010a). In mice the cycle of seminiferous epithelium is divided into 12 stages (I-XII) and spermiogenesis into 16 steps based on the spermatid development (Ahmed & de Rooij 2009). Figure 2 illustrates the specific stages and associated cell types in mice.

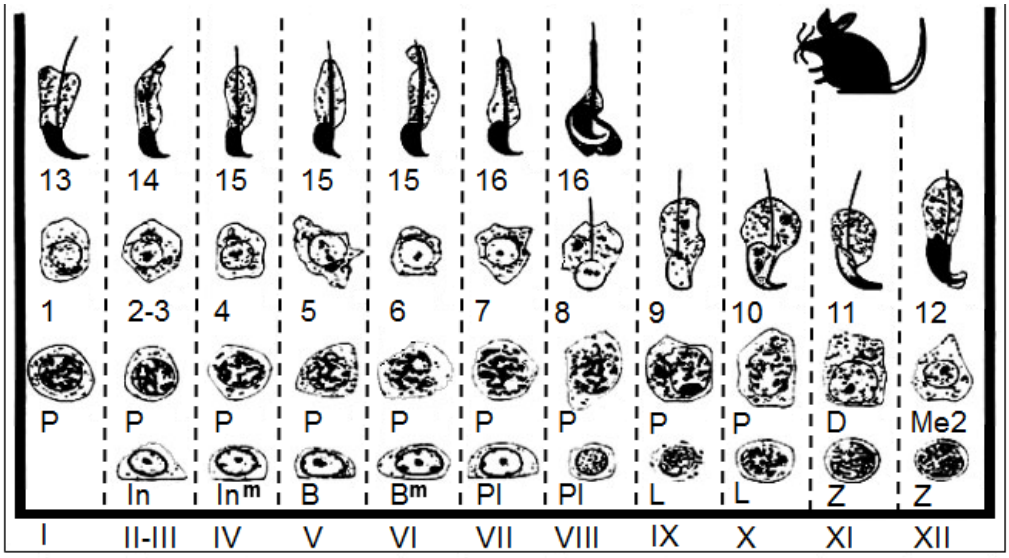

Figure 2. Schematic diagram of the cycle of seminiferous epithelium in mice. Spermatogenesis is divided into 12 stages based on the cell content of seminiferous epithelium. The 12 stages are denoted with roman numerals. Spermiogenesis, is divided into 16 steps based on spermatid development (Hess & de Franca 2008, Ahmed & de Rooij 2009). The 16 steps are denoted with Arabic numerals. In = Intermediate spermatogonium; In^m = Intermediate spermatogonium undergoing mitosis; B = type B spermatogonium; B^m = type B spermatogonium undergoing mitosis; Pl = preleptotene spermatocyte; L = leptotene spermatocyte; Z = zygotene spermatocyte; P = pachytene spermatocyte; D = diplotene spermatocyte; Me2 = a secondary spermatocyte undergoing meiosis II at the stage XII. The figure is modified from the Russell et al. (1993).

1.2.5 Sertoli cells

Sertoli cells provide structural and nutritional support for the germ cells throughout spermatogenesis (Xiao et al. 2014). The hormones excreted by Sertoli cells and Leydig cells maintain optimal environmental conditions for differentiating germ cells (Hermo et al. 2010a). Sertoli cell´s nucleus is localized near the basement membrane while its cytoplasm is spread to envelope the developing germ cells (Xiao et al. 2014) . Sertoli cells are responsible for germ cell transport across the seminiferous epithelium and successful spermiation process (Xiao et al. 2014). Elongating spermatids and Sertoli cells are connected with a specialized junction containing F-actin filaments sandwiched between Sertoli cell plasma membrane and underlying endoplasmic reticulum called apical ectoplasmic specialization (apical ES) (Vogl et al. 1991). Functional apical ES assembly and disassembly are prerequisites for a successful spermiation (Berruti & Paiardi 2014).

1.3 Spermiogenesis

Correct morphology of sperm is important for male fertility. The elongating spermatid is structurally divided into two main parts: the sperm head and sperm tail. A cell membrane covers the whole cell including the tail. Connecting piece, which contains the basal body, connects the tail to the sperm head. The elongated head consists of the acrosome and condensed nucleus. A transient manchette appears during the spermatid elongation, but vanishes before spermiation. The formation of manchette and acrosome together with nucleus condensation are the key factors in shaping the sperm head as seen in mouse models with mutations affecting any of these structures (Kierszenbaum et al. 2007)

1.3.1 The acrosome

As reviewed by Buffone et al. (2008) the acrosome is a lysosomal structure on the tip of the sperm head. It is formed in early spermatid from proacrosomic granules derived from the Golgi apparatus. The acroplaxome serves as a docking site for the granules to localize and fuse (Kierszenbaum et al. 2004). Acroplaxome is subacrosomal F-actin-keratin containing cytoskeletal plate that facilitates the acrosome biogenesis and anchors the acrosome to the nuclear envelope (Kierszenbaum et al. 2003). The marginal ring stabilizes the acroplaxome structure (Kierszenbaum et al. 2003). The proacrosomal granules continue to fuse together resulting in a single, large granule, an acrosomal sac. After binding to the nuclear envelope of round spermatids it grows in size to envelope the nucleus of elongating spermatids. At the final steps of spermatid development the acrosome has grown to cover two-thirds of the nucleus (Hermo et al. 2010b). The acrosome has an important role in the successful fertilization of an oocyte (Buffone et al. 2008). Acrosome enables the sperm to bind and penetrate into a glycoprotein layer around oocytes (zona pellucida) by activating the acrosomal reaction (Yanagimachi 2011). During acrosomal reaction the outer acrosome membrane fuses with the oocyte plasma membrane and releases enzymes and other acrosomal material needed for the sperm to penetrate into the oocyte (Yanagimachi 2011).

1.3.2 The manchette

As reviewed by Kierzenbaum and Tres (2004) the manchette is a sperm-specific filamentous actin (F-actin) containing microtubular structure. Manchette is known to be involved in nuclear shaping and additionally work as storage and transport platform for structural molecules needed for head condensation and sperm tail assembly (Kierszenbaum 2001). Moreover, manchette has been associated with the movement of residual cytoplasm to the distal side of spermatid and as a result facilitating the eventual residual body removal during the spermiation (Toshimori & Ito 2003). The manchette is formed at the caudal site of early elongating spermatids (step 9 in the mouse) and vanishes after the condensation and elongation of the sperm nucleus is near its completion (step 14) (O'Donnell & O'Bryan 2014).

Manchette has been postulated to have an important role in the sperm tail assembly and transferal of cytosol-derived protein and Golgi-derived vesicle cargo between the cell body and basal body (Kierszenbaum & Tres 2004). Mobilization of molecules along the microtubular or F-actin tracks within the manchette is called intramanchette transport (IMT) (Figure 3 (2.1) and (2.2)). IMT shares many molecular similarities with intraflagellar transport (IFT) system including the microtubule-based molecular motors, kinesin and dynein, and some of the IFT particles (Kierszenbaum 2002a). The Golgi-derived vesicles and cytosol-derived protein cargo are mobilized along the manchette microtubules with kinesin and dynein molecular motors, whereas the F-actin based vesicle pathway utilizes myosin (Figure 3 A and B) (Kierszenbaum & Tres 2004).

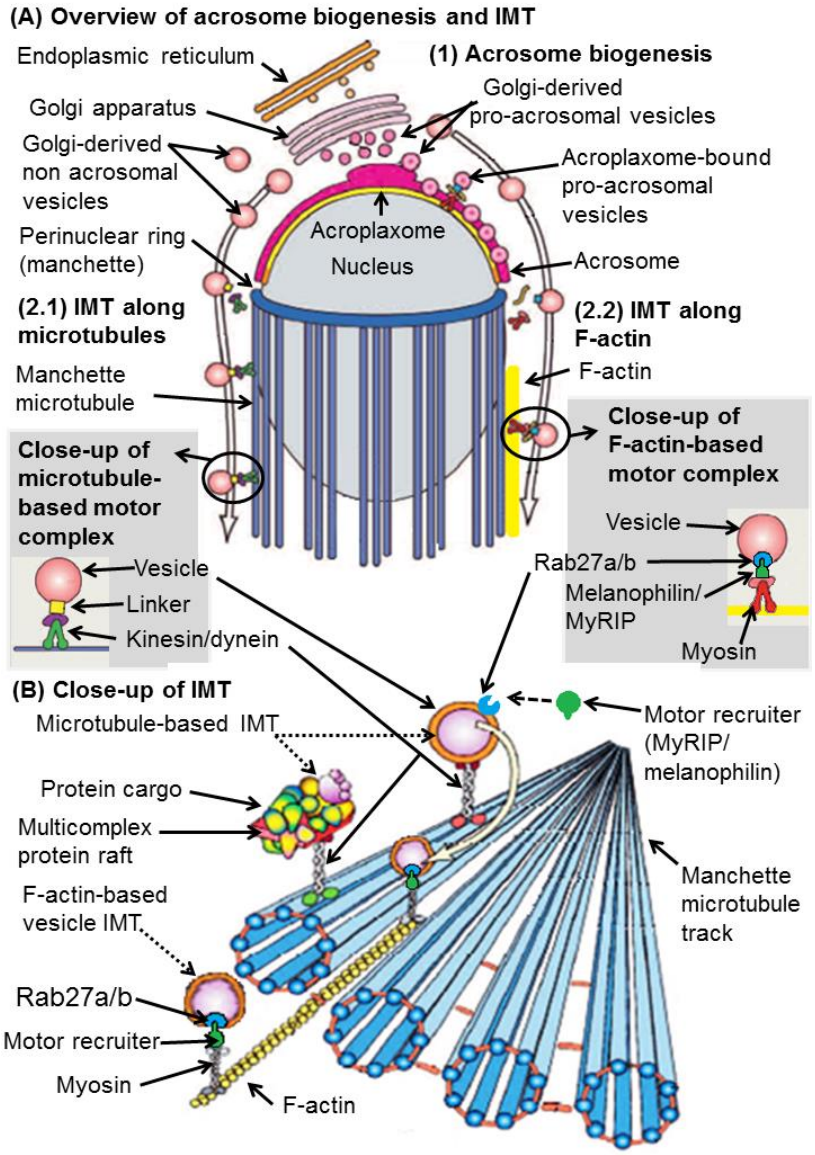

Figure 3. (A) Schematic diagram of acrosome biogenesis and IMT. (1) The acrosome biogenesis vesicle pathway includes the vesicle transport from the endoplasmic reticulum to the Golgi apparatus and from the Golgi to the acroplaxome. The Golgi-derived pro-acrosomal vesicles bind to the acroplaxome and fuse to create the acrosome. In addition to acrosome biogenesis the Golgi apparatus generates vesicles for the manchette and the sperm tail assembly. These vesicles can be transported along the manchette via two pathways: microtubule tracks of (2.1) and F-actin tracks of IMT (2.2). The microtubule-based motor complex includes molecular motor (kinesin/dynein) and linker protein carrying the vesicle along the microtubule (grey background on the left). F-actin-based motor complex is thought to include molecular motor (myosin), motor recruiter (myRIP/melanophilin) and Rab27a/b protein (grey background on the right). . (B) A close up of IMT: Cytosol-derived protein cargo on multicomplex protein rafts and the Golgi-derived vesicles can be transported along the microtubule-based tracks. Motor recruiters of F-actin-based vesicle IMT, MyRIP or melanophilin, might be regulating the switch between the two tracks (white arrow). Figures A and B are modified from Kierszenbaum and Tres (2004).

1.3.3 Shaping the sperm head

In mice the head elongation starts at step 9 during the latter half of spermiogenesis (Russell et al. 1991). The acroplaxome, manchette and successful DNA condensation are considered to be the key elements in head elongation (Borg et al. 2010). According to the model by Kierszenbaum and Tres (2004) spermatid head shaping is a result of coordinated actions of Sertoli cells and acrosome-acroplaxome-manchette complex (Figure 4). Acroplaxome binds the acrosome to the nuclear envelope. The manchette surrounds the bottom half of nucleus below the acrosome- acroplaxome complex. The area between marginal ring of the acroplaxome and perinuclear ring of the manchette is called groove belt (Figure 4). Sertoli cell's apical ES creates a clutching force from the outside of spermatid via F-actin hoops that surround the axoplaxome covered nucleus. The length of F-actin hoops is progressively being shortened during the spermatid elongation. Simultaneously, the marginal ring of axoplaxome and perinuclear ring of the manchette decrease their diameter while descending along the elongating spermatid nucleus. This generates a clutching force from within the spermatid. Furthermore, the acroplaxome may further facilitate the spermatid head elongation by transforming the exogenous clutch force generated by Sertoli cell's F-actin hoops into steadier and gentler constriction force. Similarly the manchette functions like a corset around the elongating nucleus. (Kierszenbaum & Tres 2004)

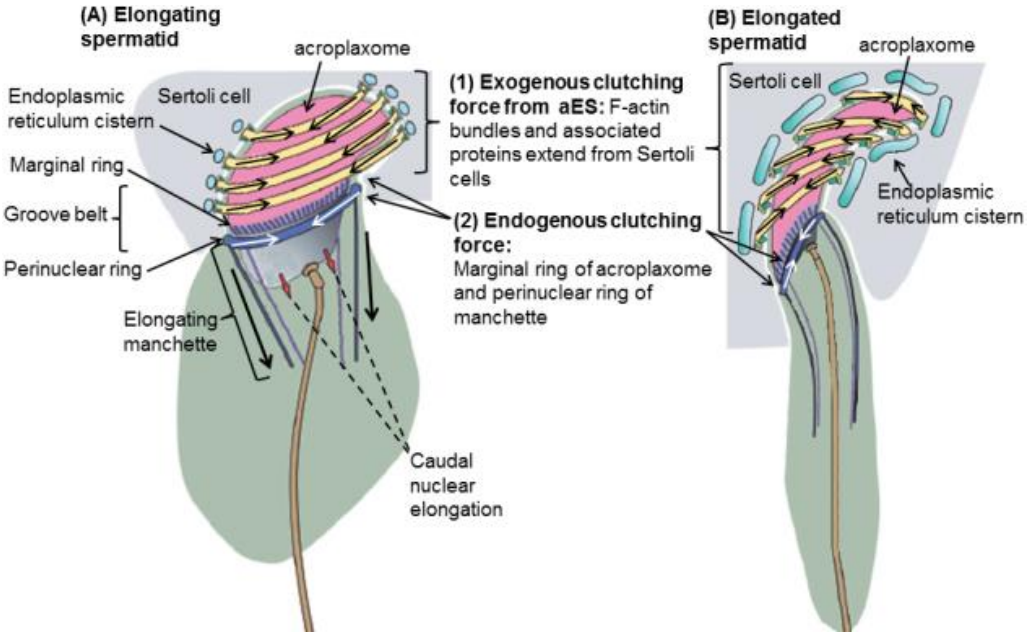

Figure 4. Schematic diagram of the sperm head shaping model. Endogenous and exogenous clutching forces steer the elongation of spermatid head in unison. (1) Exogenous clutching force: Sertoli cell derived F-actin hoops from the apical ES progressively constrict the condensing nucleus. (2) Endogenous clutching force: Marginal ring of acroplaxome and the perinuclear ring of manchette both gradually shrink while descending along the spermatid nucleus. The figure is modified from Kierzenbaum and Tres (2004).

1.3.4 Assembly and structure of the sperm tail

The sperm tail is structurally divided into four parts: the connecting piece, midpiece, principal piece and end piece. The connecting piece binds the tail to the implantation fossa of the nucleus (Turner 2003, O'Donnell & O'Bryan 2014). The basal body, formed from the centriole, resides in the connecting piece and facilitates the axoneme formation (Turner 2003). Axoneme is a microtubules-based cytoskeleton present in the sperm and cilia (Ibanez-Tallon et al. 2003). The axonemal structure of sperm tail is of 9+2 configuration in which a ring of nine doublet microtubules surround two central microtubules (Ibanez-Tallon et al. 2003). The outer doublet microtubules are comprised of one complete microtubule (the A tubule) and one with fewer protofilaments (the B tubule) (Ishikawa & Marshall 2011). The most numerous proteins found in the axoneme are the α- and β-tubulins, which form dimers for assembly of microtubule protofilaments (Kierszenbaum 2002b, Turner 2003). The sperm tail axoneme includes dynein arms that create the movement and various accessory structures that regulate the bend of the sperm tail (Turner 2003).

The centrosome localization next to the nucleus of round spermatid initiates the formation of the connecting piece and axoneme (Goto et al. 2010, O'Donnell & O'Bryan 2014). The centrosome is comprised of a pair of centrioles denoted as distal and proximal centrioles (Goto et al. 2010). The centrosome is surrounded by pericentriolar matrix (PCM) at which the gamma-tubulin resides as a part of gamma-tubulin ring complexes (γ-TuRCs) (O'Donnell & O'Bryan 2014). In rodents both of the centrioles are degenerated from the mature sperm in a process termed centrosome reduction (Manandhar et al. 1999). In mice the distal centriole is lost already in the testis during spermiogenesis whereas the proximal centriole disappears during the epididymal stage of sperm cell maturation (Manandhar et al. 1998). The loss of PCM proteins such as gamma-tubulin occurs prior to the reduction of distal centriole (Manandhar et al. 1999). During the spermiation gamma-tubulin is casted off into the residual bodies (Manandhar et al. 1998).

In addition to the axoneme, mammalian sperm tail includes three additional accessory structures: the mitochondrial sheath (MS), outer dense fibers (ODFs), and fibrous sheath (FS) (Turner 2003) (Figure 5 B). The thickest part of the tail, midpiece, ranges from the end of connecting piece to the ring-shaped annulus (Figure 5 A). The annulus is a septin containing membrane diffusion barrier between midpiece and the principal piece (Kwitny et al. 2010). The axoneme in the midpiece is surrounded by 9 ODFs and MS (Figure 5 B). ODFs provide support for the tail and the MS the energy needed for the tail movement (Turner 2003). In the principle piece two of the ODFs are replaced

by longitudinal FS columns (Figure 5 B). Circumferential transverse ribs (TR) bind the two FS columns together (Figure 5 B). As well as providing mechanical support for the tail, FS is associated with many signaling and metabolic cascades needed for sperm motility (Turner 2003). In the most distal and shortest part of the tail, end piece, the axoneme is only surrounded by the sperm tail membrane (Figure 5 B).

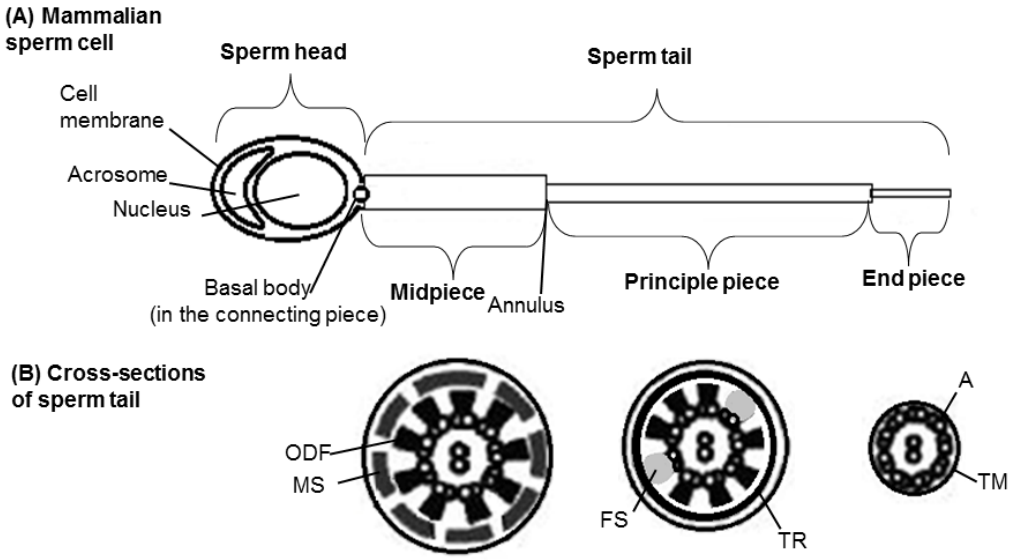

Figure 5. (A) Schematic diagram of mammalian sperm cell. The sperm cell can be structurally divided into two parts: sperm head and tail. The sperm head is mostly comprised by the acrosome and condensed nucleus. Tail has four distinctive pieces: the connecting piece, midpiece, principal piece and end piece. The basal body resides in the connecting piece and nucleates the axoneme. The connecting piece attaches the tail to the nucleus. (B) Cross-sections of the midpiece, principle piece and end piece. The axoneme in the midpiece is surrounded by nine outer dense fibers (ODF) and mitochondrial sheath (MS). The midpiece extends from the connecting piece to the annulus. In the principle piece two of the ODFs are replaced by longitudinal fibrous sheath (FS) columns which are connected by circumferential transverse ribs (TS). In the end piece only the axoneme (A) and tail membrane (TM) remain. Figure is modified from Lehti et al. (2013).

The formation of additional accessory structures is initiated after the axoneme assembly starting with the FS. In mice the longitudinal columns of the FS begin to form at the step 9 (Turner 2003, Hu et al. 2009). The formation of ODFs is initiated after the FS (Horowitz et al. 2005). The formation of MS begins after the migration of annulus to the proximal end of FS during steps 14-15 (Ho & Wey 2007). The annulus is first formed in the connecting piece and subsequently migrates to the most proximal end of FS (Turner 2003). Axoneme, MS and ODFs are constructed from the proximal end to the distal end of the sperm tail whereas the FS is formed in opposite direction from distal tip of the principle piece towards the annulus of midpiece (Turner 2003).

1.3.5 IFT

Since cilia lack protein synthesis machinery of their own they are dependent on the IFT system that shuffles essential proteins and other molecules from the cell body to ciliary tip (anterograde transport) and from the cilia back to cell body (retrograde transport) (Cardenas-Rodriguez & Badano 2009) (Figure 6). Molecular motors move vesicle and protein cargo along the microtubules (Rosenbaum & Witman 2002). Generally kinesin II is used in anterograde transport and dynein in retrograde transport (Rosenbaum & Witman 2002). Kinesin II is a heterotrimeric protein complex formed from 2 motor subunits (KIF3A and KIF3B) and KAP3 subunit (Scholey 1996a, Scholey 1996b). Dynein, the retrograde molecular motor, is macro-molecular complex formed by two heavy chains and various subunits (O'Donnell & O'Bryan 2014). Molecular motors are connected to multiprotein complexes denoted as IFT particles (Rosenbaum & Witman 2002). IFT particle contains two subcomplexes with different protein components: IFT complex B and IFT complex A (Rosenbaum & Witman 2002). IFT complex A participates in the retrograde IFT and IFT complex B in the anterograde IFT (Ishikawa & Marshall 2011). IFT is pivotal for formation, maintenance and function of cilia and sperm tails (Cardenas-Rodriguez & Badano 2009). Deleterious mutations affecting the IFT such as loss of function mutation in KIF3A are known to result in abnormal cilia and sperm tail formation and function (Cardenas-Rodriguez & Badano 2009, Lehti et al. 2013).

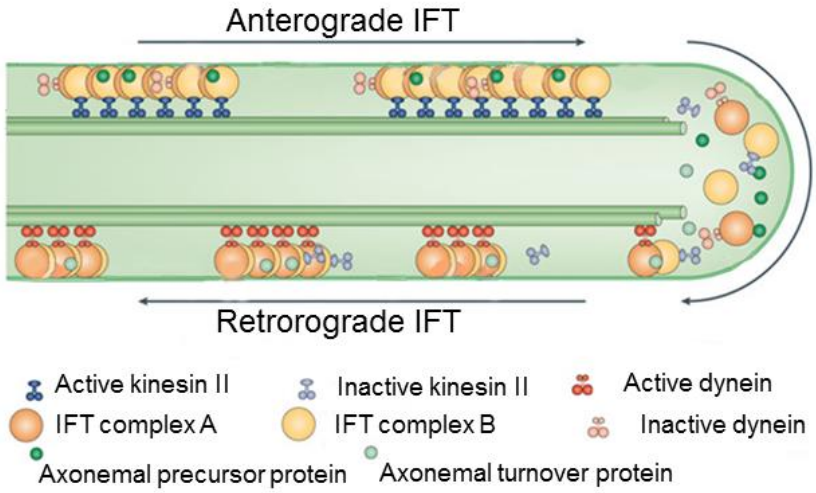

Figure 6. Schematic diagram of IFT in cilia. Molecular motors transport vesicles and protein rafts along microtubule tracks of the axoneme. Kinesin II can only move from the cell body to the tip of cilium (anterograde) and dynein from cilium tip to the cell body (retrograde) thus kinesin II must carry inactive dynein to the cilium tip and dynein carries the inactivated kinesin II back to the basal body region. The multiprotein complexes connected to molecular motors are denoted as IFT particles. IFT particle consists of two subcomplexes with different protein components: IFT complex B and IFT complex A. Diagram is modified from Ishikawa and Marshall (2011).

1.4 Sperm flagellar protein 2 (SPEF2)

A correct sperm tail formation and maintenance is needed for sperm motility and loss of it can cause male infertility. Sperm flagellar protein 2 (SPEF2 also known as KPL2) is known to be essential for the assembly of sperm tail and male fertility in pigs and mice (Sironen et al. 2006, 2011). The gene coding for SPEF2 is highly conserved in mammals and belongs to the SPEF protein family together with SPEF1 (Sironen et al. 2011). *Spef2* was first discovered by Ostrowski et al. (1999).Their research group was searching for novel genes induced during ciliogenesis of tracheal epithelial cells of rat. In the same study a stage-specific expression of SPEF2 during spermatogenesis was reported. The pivotal role of *Spef2* in spermatogenesis was not fully understood until an intronic insertion of LINE-1 retrotransposon into *Spef2* gene was indicated to cause the immotile short-tail sperm defect (ISTS) in Finnish Yorkshire boars (Sironen et al. 2006, 2007). SPEF2 has been suggested to participate in IFT after the discovery of known IFT complex B protein, IFT20, as an interaction partner for SPEF2 by Sironen et al. (2010). The importance of SPEF2 in spermatogenesis got further validation after the discovery of a nonsense mutation within *Spef2* in big giant head mice (bgh mice) (Sironen et al. 2011). The loss of SPEF2 function was shown to disrupt the sperm tail formation and the beat frequency of motile cilia resulting in common symptoms associated with the primary cilia dyskinesia: hydrocephalus, mucus accumulation and male infertility (Sironen et al. 2011, Finn et al. 2014).

SPEF2 has been predicted to have five extremely conserved domains among mammalian species (DUF1024, CH, ADK, P-loop and EF-hand; Figure 7). DUF1042 domain of unknown function is located in the N terminus of SPEF2 (Sironen et al. 2006). Interestingly, DUF1042 domain is shared with other proteins associated with sperm tail such as SPEF1 (mouse sperm flagellar protein 1) and CPC1 (central pair complex 1 of *Chlamydomonas reinhardtii*). Additionally, SPEF2 has been reported to have a calponin homology (CH) domain with a potential actin-binding activity (Sironen et al. 2006). Therefore, it was suggested that SPEF2 might have an additional role in regulating the actin dynamics in spermatogenesis (Sironen et al. 2010). F-actin is known to be involved in IMT, spermiation and the germ cell transport across the seminiferous epithelium via apical ES (Kierszenbaum & Tres 2004, Xiao et al. 2014). Moreover, actin is involved in phagocytosis of cytoplasmic debris left behind from the spermatid elongation and in phagocytosis of retained sperm and apoptotic germ cells by Sertoli cells (Clermont et al. 1987, Otsuka et al. 2009). In addition to CH domain, SPEF2 is estimated to have an adenylate kinase (ADK) and P-loop domain potentially acting as an ATP/GTP binding site (Sironen et al. 2006). The C terminus of SPEF2

contains an EF-hand motif with calcium-binding ability, which has been suggested to implicate a calcium regulated activity for SPEF2 (Sironen et al. 2006).

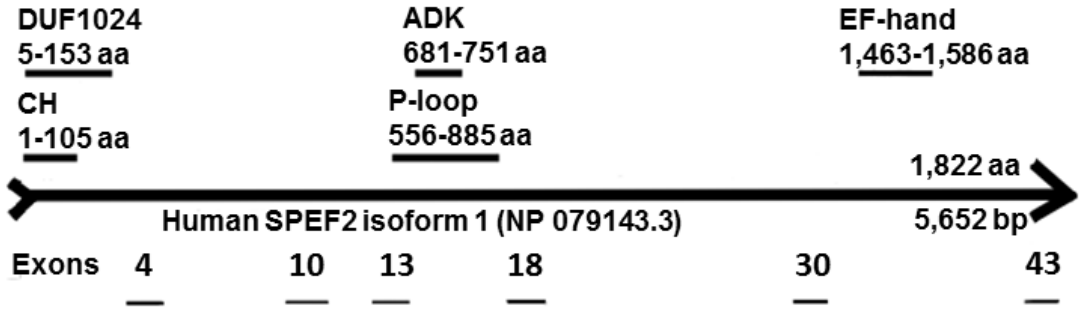

Figure 7. An overview of human SPEF2 isoform 1 (denoted as NP 079143.3 in the National Center for Biotechnology) and its predicted functional domains. The human SPEF2 isoform 1 is transcribed from 43 exons and consists 1,822 amino acids. SPEF2 isoform 1 is predicted to have 5 functional domains conserved among mammalian species (DUF1024, CH, ADK, P-loop and EF-hands) (Sironen et al. 2006). DUF1042 is a sperm tail associated domain of an unknown function located in the N-terminus of SPEF2 (Sironen et al. 2006). SPEF2 also contains a CH domain (calponin homology) with a potential acting binding ability and an adenylate kinase (ADK) domain (Sironen et al. 2006). Furthermore, SPEF2 is predicted to contain a P-loop motif (potential ATP/GTP binding site) and a calcium binding EF-hand motif (Sironen et al. 2006). Predicted domains are depicted with black bars and the exons with black lines. The figure is modified from Sironen et al. (2010).

1.5 Aims of the study

Although it is known that the impaired *Spef2* function causes infertility (Sironen et al. 2006, 2011, Finn et al. 2014), the concrete role of the SPEF2 protein in the spermatogenesis is yet to be confirmed. It has been suggested that SPEF2 may contribute to the sperm tail assembly as a part of IFT system (Sironen et al. 2010, Sironen et al. 2011). The aim of my master thesis is to investigate the role of this protein in the spermatogenesis by using an unpublished male germ cell specific conditional knock out (Spef2 cKO) mouse model and novel anti-SPEF2 antibodies.

The specific aims of the study are:

1. To characterize the phenotype of Spef2 cKO mouse model.
2. To test the functionality of novel anti-SPEF2 antibodies using Spef2 cKO model as a negative control.

2 Materials and Methods

2.1 Animal material

Spef2 cKO (Ngn3Cre; Spef2 FL) is a germ cell specific conditional knockout mouse model created with Cre-Lox recombination technique. In this mouse model Cre recombinase is controlled by spermatogonia specific neurogenin 3 (Ngn3) promoter and as a result is only activated in the germ cells of male mice. The activated Cre recombinase targets the LoxP sites surrounding exons 3- 5 of *Spef2* gene. Only the male mice who have inherited the Cre recombinase and the LoxP sites (Ngn3Cre+; Spef2 FL/FL) express the knockout phenotype and are therefore infertile due to lack of SPEF2 protein. The Ngn3-Cre mouse line and used technique in creating a male germ cell conditional mouse model have been described by Korhonen et al. (2011).

2.2 Genotyping

Two weeks old mice were earmarked and ear samples were collected and sent to the former MTT (Agrifood Research Finland) for DNA isolation and genotyping. The genotyping was carried out by PCR. Genotyping was performed using the following PCR primers: Sense primer was Spef25Armse4 GATTCTTAAATTTTGAGGCC and the antisense primer was Spef25ArmDR3 ATGCTGTTCAGTGGATAAAA. Based on the genotyping results mice were selected for further analysis.

2.3 Tissue collection and preservation

Mice were sacrificed with CO2. Testis and epididymis tissues from WT and Spef2 cKO mice were collected and processed for experiments as required using specific protocols described below.

2.4 Drying down (DD) preparations

The testes were collected from WT and Spef2 cKO mice in PBS (pH 7.2-7.4). Stage-specific segments of seminiferous tubules (II-V, VII-VIII and IX-XI) were identified (Kotaja et al. 2004) and transferred in 100mM sucrose solution. The cells were released and fixed on slides with fixative (1% PFA and 0.15% Triton-X-100 in PBS; pH 9-9.2). The slides were incubated overnight in humidified chamber. The following morning the slides were air-dried, washed twice with 0.2 % Triton-X-100 in PBS and dried at RT. DD-samples were stored at -80 °C.

2.5 Cryo-sections

Testes were collected from adult WT and Spef2 cKO mice and embedded with Tissue-Tek OCT (Sakura Finetek) and frozen with isopentane (cooled by dry ice). The block was sectioned with Leica CM 3050 and dried at RT after which the cryo-sections were stored in -80 °C.

2.6 Paraffin embedded tissues

2.6.1 Fixing testis and epididymis with paraformaldehyde or Bouin solution

Testes and epididymides were collected from adult WT and Spef2 cKO mice and fixed with 4% paraformaldehyde (PFA) or Bouin solution for 4 h at RT in rotation. PFA solution was changed and left to fix overnight. The following day the PFA-fixed tissues were washed with 50% EtOH (2x30 min), 70% EtOH (2x30 min) and stored in 70% EtOH at +4 °C until embedded with paraffin. Bouin fixed testes were washed under running water for 1-2 h and then with 70% EtOH (2x30 min) at RT in rotation. The 70% EtOH wash was repeated until the yellow colour from Bouin solution disappeared completely and stored in 70% EtOH at +4 °C until embedded with paraffin.

2.7 Immunofluorescence

2.7.1 Paraffin-embedded testis sections

Paraffin-embedded testis sections were cut and deparaffinized with xylene (3x5 min). The sections were then rehydrated by washing with alcohols of decreasing concentration (2x5 min in 100% EtOH, 2x5 min in 96% EtOH and 2x5 min in 70% EtOH). Before antigen retrieval they were rinsed with dH2O (1x2 min). Antigen retrieval was done by pressure cooker treatment (20 min at the boiling temperature and 2 h in the leftover heat) in Sodium Citrate buffer (0.05% Tween20 in 10 mM Sodium Citrate; pH 6.0). The sections were then washed with dH2O 4x3 min and PBS 1x3 min. To block any unspecific sites the sections were incubated for 1 h with a block solution (3 % BSA, 10 % NGS and 0.1% Tween20 in PBS) inside a humidified chamber at RT. After blocking the sections were incubated overnight inside a humidified chamber at +4 °C with various anti-SPEF2 antibodies (Kad, GS-Spef2, Abnova and Sigma). The antibodies were diluted into dilution buffer (1% BSA, 3% NGS and 0.1% Tween20 in PBS). The following day the sections were rinsed with 0.1% Tween20 in PBS 3x5 min and incubated with Alexa Fluor 594 Goat anti-Rabbit IgG or Alexa Fluor 594 Goat anti-Mouse IgG (Molecular Probes) diluted in 1:500 with a dilution buffer for 1 h inside a humidified chamber protected from the light at RT. The sections were then rinsed with

0.1% Tween20 in PBS 3x3 min and PBS before the nuclear staining with DAPI (Sigma) diluted in 1:10 000 with PBS (5 min). Before mounting the sections with Vectashield HardSet (Vector Laboratories) they were rinsed with 0.1 % Tween20 in PBS 3x3 min and PBS. The stainings were visualized with Zeiss AxioImager or Leica DMRBE microscope.

To study the phenotype of Spef2 cKO mice paraffin embedded testis sections were stained with anti-acetylated alfa-tubulin, anti-gamma-tubulin, PNA, Espin antibody or HPA. Apart from using 0.1% Triton-X-100 in the place of Tween20 and 5% propyl gallate with Mowiol as a mounting medium the stainings were done with the same paraffin-embedded testes section procedure than anti-SPEF2 antibody stainings. The primary antibodies were anti- acetylated alfa-tubulin antibody diluted in 1:1500 (Sigma), anti-gamma-tubulin antibody (T7451, Sigma) diluted in 1:1000 and anti-Espin-antibody (BD Biosciences) diluted in 1:1000. The following day the sections were incubated with Alexa Fluor 488 Goat anti-Mouse IgG (Molecular Probes) diluted in 1:500 with the dilution buffer (1% BSA, 3% NGS and 0.1% Triton-X-100 in PBS) for 1 h inside a humidified chamber protected from the light at RT. The sections with anti-Espin staining were additionally incubated with rhodamine labeled peanut agglutinin (PNA, RL-1072, Vector Laboratories) diluted in 1:5000 with PBS (20 min) after the secondary antibody. Nuclei were visualized with DAPI. The immunofluorescence stainings were visualized with Leica DMRBE microscope.

The HPA staining was done with the standard paraffin-embedded testes section procedure. After the incubation with the blocking solutions the sections were incubated with a Lectin Helix pomatia agglutinin (HPA) Alexa Fluor 488 conjugate (Molecular probes) diluted in 1:50 with PBS (20 min) and washed with PBS (3x5 min) before the nuclear staining with DAPI. The sections were washed with PBS (2x5 min) and mounted with Mowiol with 5% propyl gallate. The staining was visualized with a Zeiss AxioImager microscope.

2.7.2 Optimization of the anti-SPEF2 staining

Since the standard staining procedure did not work properly I tried to optimize the procedure by using longer deparaffinization time with xylene (3x10 min), longer dehydration times with alcohol treatment (2x10 min in 100% EtOH, 96% EtOH and 70% EtOH), stronger washing dilutions (0.2%-0.3% Triton-X-100 in PBS) and longer washing times (from 5 min to 10 min), stronger blocking dilutions (10% BSA, 10% NGS and 0.1% Triton-X-100 in PBS) and stronger antibody dilution buffers (3% BSA, 10% NGS and 0.1% Triton-X-100 in PBS) and different dilutions of anti-SPEF2 antibodies

(1:500-1:10 000 for Kad; 1:500-1:5000 for GS-Spef2, 1:500-1:2000 for Abnova) and different Alexa Fluor secondary antibodies (Molecular Probes).

2.7.3 Cryo-sections

Cryo-sections were fixed with 4% PFA (5 min), washed with 0.1% Tween20 in PBS (3x3 min). Permeabilization was carried out with 0.2% Triton-X-100 in PBS (5 min). The sections were washed with 0.1% Tween20 in PBS (3x3 min) and incubated with the blocking solution (3% BSA and 5% NGS in PBS) for 2 h at RT. The sections were then incubated with one of the anti-SPEF2 antibody dilutions in blocking solution overnight inside a humidified chamber at +4 °C. Cryo-sections were stained with an anti-SPEF2 antibody (Kad 1:1000 & 1:500, GS-Spef2 1:1000 & 1:500, KPL2end 1: 500 & 1:250, Sigma 1:1000 or Abnova 1:1000). The following morning the sections were washed with 0.1% Tween20 in PBS (3x3 min) and incubated with Alexa Fluor 594 Goat anti-Rabbit IgG or Alexa Fluor 594 Goat anti-Mouse IgG diluted in 1:500 with blocking solution for 1 h at RT. The sections were washed with PBS (3x3 min) before the nuclear staining with DAPI diluted in 1:5000 with PBS (5 min). Before mounting sections with Mowiol or Vectashield HardSet they were washed with PBS. The staining was visualized with a Zeiss Axiolmager microscope.

2.7.4 Drying down samples

Drying down samples were fixed with 4% PFA (5 min) and washed with PBS (3x3 min). The sections were then rinsed with 100 mM Ammonium chloride (1x2min) and washed with PBS (1x3min) before the permeabilization with 0.2% Triton-X-100 in PBS (1x2 min). The samples were washed with PBS (3x3 min) and incubated with a blocking solution (1% BSA, 3% NGS and 0.1% Triton-X-100 in PBS) for 1 h at RT. The samples were incubated with Kad (1:500), GS-Spef2 (1:500) or anti-alfa-tubulin antibody (NeoMarkers, 1:2000) overnight at +4 °C. The antibodies were diluted with the blocking solution. The following morning the samples were washed with 0.1% Triton-X-100 in PBS (3x3 min) and incubated with Alexa Fluor 488 Donkey anti-Mouse IgG or 594 Donkey anti-Rabbit IgG (Molecular Probes) diluted in 1:500 with the blocking solution for 1 h at RT. The samples were washed with 0.1% Triton-X-100 in PBS (3x3 min) and rinsed with PBS before the nuclear staining with DAPI (Sigma) diluted in 1:10 000 with PBS (5 min). The samples were washed with 0.1% Triton-X-100 in PBS (3x3 min), rinsed with PBS and mounted with 5% propyl gallate with Mowiol. The staining was visualized with Leica DMRBE microscope.

2.8 Hematoxylin and Eosin staining (HE staining)

Bouin fixed testis sections and PFA fixed epididymis sections were cut and deparrafinized with xylene (3x5 min) and rehydrated by alcohol treatment (dip and 5 min rinse in 100% EtOH; dip and rinse in 96% EtOH and dip and rinse in 70% EtOH). The sections were rinsed three times with dH2O and stained with Delafield's Hematoxylin (HistoLab) for 15 min. The sections were rinsed twice quickly and once for 10 min in dH2O. The differentiation was done with acid alcohol treatment (70% EtOH in 2.5 mL HCl) for 1 min. The sections were washed twice quickly and once for 10 min in dH2O before the eosin staining (Reagena) for 2 min. The sections were rinsed twice with 100% EtOH and with xylene (2x5 min). The sections were then mounted with PERTEX (HistoLab). Testis and epididymis sections were visualized with Leica DMRBE microscope.

2.9 Identification of specific stage groups

In this study the specific stages of cross-sections of seminiferous tubules of WT mice were compared with the corresponding stages of Spef2 cKO mice to characterize the Spef2 cKO mouse model. Similarly, in anti-SPEF2 antibody testing the corresponding groups of stages were compared between WT and Spef2 cKO mice. Therefore, the correct identification of specific stage groups in cross-sections was important.

In mice the spermatogenesis can be divided into 12 stages. During stages II-V the bundles of elongating spermatids are formed (Figure 8 A and B). During the following stages VI-VII elongated spermatids are released from the bundles and transported to the edge of lumen by Sertoli cells (Figure 8 C). In the stage VIII-IX elongated spermatids have been released to lumen while spermatocytes and round spermatids have remained behind (Figure 8 D). In the subsequent stages X-XI round spermatids have turned into elongating spermatids (Figure 8 E). During the stage XII the second meiosis takes place and a new generation of round spermatids are formed (Figure 8 F).

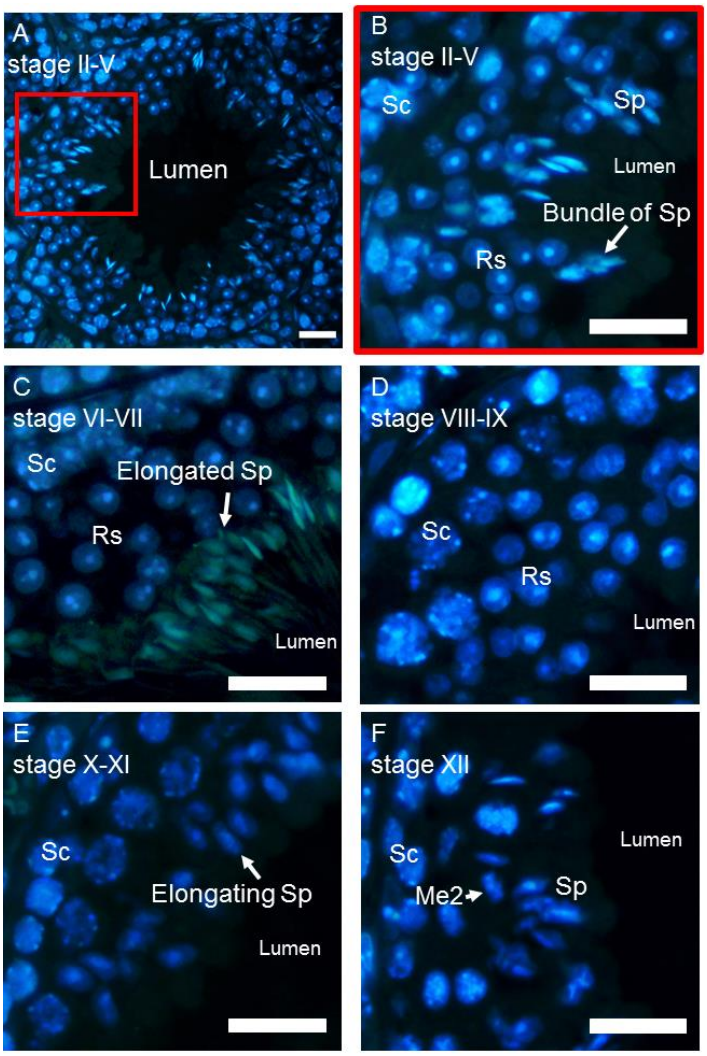

Figure 8. Paraffin-embedded cross-sections of seminiferous tubules of WT mouse stained with nuclei staining DAPI (blue). (A) An overview of the stage II-V cross-section. (B) A close up of Figure A: during the stages II-V the elongating spermatids are being hold in bundles by Sertoli cells (arrow). (C) During the stages VI-VII elongated spermatids are positioned around the edge of the lumen (arrow). (D) The spermiation occurs in the stage VIII after which only spermatocytes and round spermatids can be seen in the cross-section. (E) During the stages X-XI the round spermatids are transforming into elongating spermatids (arrow). (F) In the stage XII the second meiosis (arrow) takes place and round spermatids appear at the stage I. Sc = spermatocyte; Rs = round spermatid, Sp = spermatid, Me2 = meiosis 2 The scale is 20 µm.

2.10 Western blot

Testes were collected from adult WT and Spef2 cKO mice. For protein isolation tissues were homogenized with Ultra Turrax in lysis buffer (50 mM Tris-HCl pH 8, 170 mM NaCl, 1% NP-40, 5 mM EDTA; 1 mM DTT, 0.2 M PMSF and protease inhibitors (Complete mini; Roche diagnostic)) on ice. The sample was centrifuged at 13,000 rpm for 20 min at + 4 °C and the supernatant was collected. The protein concentration was measured with Bradford protein assay (Thermo Scientific) using the protocol by the manufacturer. Two novel anti-SPEF2 antibodies (GS-Spef2 and Kad) were first tested and based on those results Kad was chosen for the following western blot experiments. Tissue lysis from the Spef2 cKO mice were used as a negative control.

The protein samples were separated in 7 % SDS-PAGE gel (Bio-Rad). Prior to the electroblotting, a polyvinylidene fluoride membrane was activated by 30 s incubation in 100% MeOH followed by 1-3 min rinse in dH_2O. The gel and the activated polyvinylidene fluoride membrane were soaked in Towbin transfer buffer for 10 minutes. The samples were electroblotted to polyvinylidene fluoride membrane for 2 h (90 V, 400 mA) on ice. The membranes were incubated with a blocking solution (nonfat 5% milk diluted with 0.1% Triton-X-100 in PBS) for 1h at RT. The membranes were incubated overnight with primary antibodies at +4 °C in rotation. The anti-SPEF2 antibodies (Kad and GS-Spef2, 1:500) were diluted in nonfat 1% milk diluted with 0.1% Triton-X-100 in PBS. The following day the membranes were washed with 0.1% Triton-X-100 in PBS (4x15 min). Antigen-antibody complexes were detected by incubating the membranes with HRP-conjugated anti-Rabbit secondary antibody (Cell signaling technologies) diluted in 1:4000 with 0.1% Triton-X-100 in PBS for 1 h at RT in rotation. The membranes were washed with 0.1% Triton-X-100 in PBS (4x15 min) and incubated with Western Lightning ECL Pro (PerkinElmer) using the protocol by the manufacturer. The chemiluminescence signal was measured using LAS4000 (Fujifilm).

The positive control was done with anti-alfa-tubulin antibody (NeoMarkers) diluted in 1:4000 with dilution buffer (nonfat 1% milk diluted with 0.1% Triton-X-100 in PBS). Prior to the anti-alfa-tubulin antibody incubation the membrane was first stripped by washing the membrane twice for 10 min with stripping buffer (2 M Tris-HCl, 0.2% NP-40 and 0.8 mL ß-mercaptoethanol in 6 M GnHCl, pH 7.5). The stripped membrane was then rinsed with 0.2% NP-40 in TBS (4x3 min) and the unspecific sites were blocked with nonfat 5% milk diluted with 0.1 % Triton-X-100 in PBS for 1h at RT in rotation. The following protocol was as described before.

3 Results

3.1 The Spef2 cKO mouse model

Spef2 cKO mouse model was created with Cre-Lox recombination technique. Spef2 cKO mice have the added LoxP-sites surrounding exons 3 and 5 within *Spef2* gene (Figure 9). Heterozygous female mice (Spef2 FL/WT) were bred with heterozygous males expressing Cre recombinase (Ngn3Cre+; Spef2 FL/WT) to produce the homozygous Spef2 FL/FL offspring (Ngn3Cre+; Spef2 FL/FL). The genotyping was done by PCR with forward and reverse primers targeting a LoxP-site (Figure 9 and 10). The loss of SPEF2 in the Spef2 cKO testis has been validated by western blot using Kpl2end as an anti-SPEF2 antibody (data not shown).

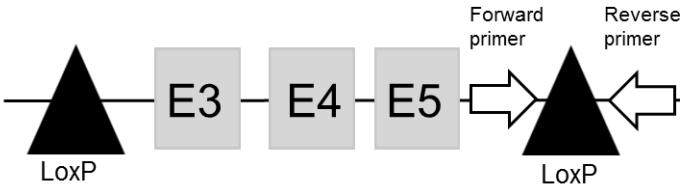

Figure 9. A schematic representation of LoxP-sites surrounding the exons 3-5 within *Spef2* gene in Spef2 cKO mouse model. Due to the deletion of the three exons within the *Spef2* gene functional SPEF2 protein is not produced. *Spef2* cKO genotype was verified by PCR using forward and reverse primers targeting a LoxP-site.

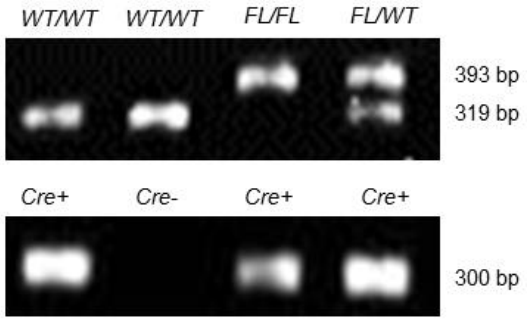

Figure 10. Genotyping results from Spef2 cKO mouse line. The predicted product sizes were as follows: for WT (319 bp), for mutant *Spef2* gene (393 bp) and for Cre+ (300 bp).

3.2 Characterization of Spef2 cKO phenotype

3.2.1 Spef2 cKO male mice are infertile

Consistent to the previous Spef2 animal models, loss of functional SPEF2 causes infertility in Spef2 cKO male mice. To visualize the content of the epididymis in the Spef2 cKO mouse model the epididymis of Spef2 cKO and WT mice were stained with hematoxylin and eosin. In WT caput and cauda sections of epididymis the amount of sperm was notably higher than in Spef2 cKO sections (Figure 11). Furthermore, sperm morphology seemed to differ between WT and Spef2 cKO (Figure 11 inserts). The few spermatozoa produced by Spef2 cKO mice had only partially formed tail or no tail at all. Moreover, in the place of sperm, a huge amount of cell debris could be observed in Spef2 cKO epididymis cauda section.

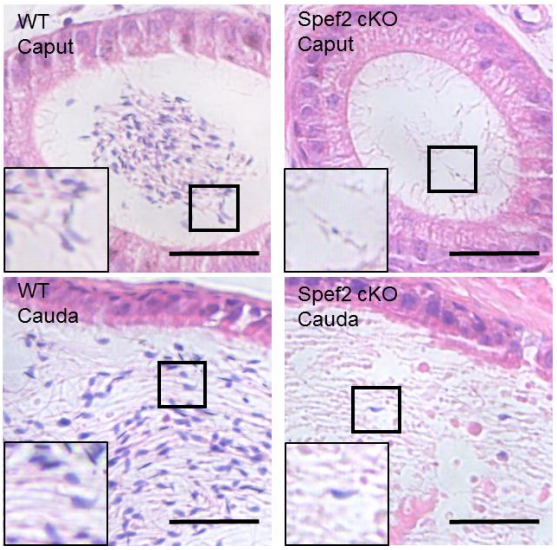

Figure 11. HE stained WT and Spef2 cKO epididymis sections. Spef2 cKO epididymis was almost void of sperm cells. The Spef2 cKO caput was virtually empty of sperm compared to WT caput. In addition, the Spef2 cKO cauda section contained significantly fewer sperm cells than WT. Moreover, the tails were either missing or only stump tails were present in Spef2 cKO epididymis (marked with black squares and an insert). The scale bar is 20 µm.

3.2.2 Loss of SPEF2 causes club-shaped sperm heads and disrupts sperm tail formation

In order to characterize the Spef2 cKO phenotype the Bouin fixed testis sections were stained with hematoxylin and eosin. In general, spermatogenesis appeared to progress

identically between WT and Spef2 cKO until spermiogenesis (Figures 12 and 13). In the beginning of spermatid elongation during the steps 8-9 the spermatid heads appeared similar between WT and Spef2 cKO testis sections (Figure 12 A and B). During the steps 9-11 the spermatid heads appeared similar between WT and Spef2 cKO testis sections (Figure 12 C and D). However retained mature sperm cells were observed in the stages IX-XI Spef2 cKO testis section, suggesting a failure in spermiation (insert in Figure 12 D). The first signs of abnormal head shaping in Spef2 cKO became evident in step 12-13 spermatids whose heads were club-shaped compared to more oval-shaped WT spermatids (Figure 12 E and F inserts). In contrast, meiosis 2 appeared to progress identically between WT and Spef2 cKO testis sections since Spef2 cKO spermatocytes were seen to successfully go through meiotic division 2 (Figure 12 E and F).

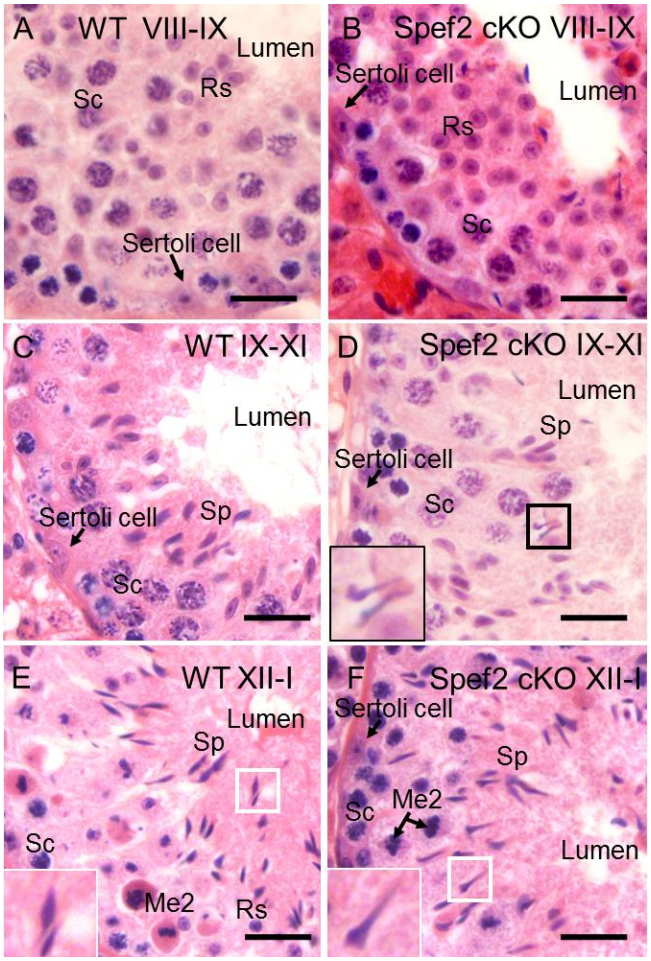

Figure 12. Loss of *Spef2* seemed to cause defects in late spermiogenesis. (A-F) HE stained WT and Spef2 cKO testis sections. (A and B) The WT and Spef2 cKO steps 8-9 round spermatids seemed identical between WT and Spef2 cKO testis sections.(C and D) The beginning of spermatid elongation (steps 9-11) appeared to progress identically between Spef2 cKO and WT. However, unlike WT testis section, Spef2 cKO contained retained sperm cells (marked with black squares and an insert). (E and F) Meiosis 2 (Me2) progressed normally in the stages XII-I Spef2 cKO testis section. In contrast, the first signs of club-shaped heads were observed to appear in

step 12-13 spermatids (marked with white squares and an insert) . The scale bar is 20µm. Sc=spermatocyte; Sp=spermatid; Rs=round spermatid

In the WT testis section of step 14-15 spermatids tails and normally developed spermatid heads could be observed (Figure 13 A). In contrast, Spef2 cKO's elongated step 14-15 spermatids had often club-shaped heads and no tails could be seen (Figure 13 B). Subsequently, the bundle formation of elongating spermatids was observed to progress similarly in WT and Spef2 cKO testis sections as the WT and Spef2 cKO spermatids were seen in similar groups (Figure 13 A and B). During the stages VI-VII Spef2 cKO testis section appeared to contain less elongated step 15-16 spermatids (Figure 13 C and D). Moreover, unlike WT testis section, no tails were observed in the Spef2 cKO testis (Figure 13 C and D).

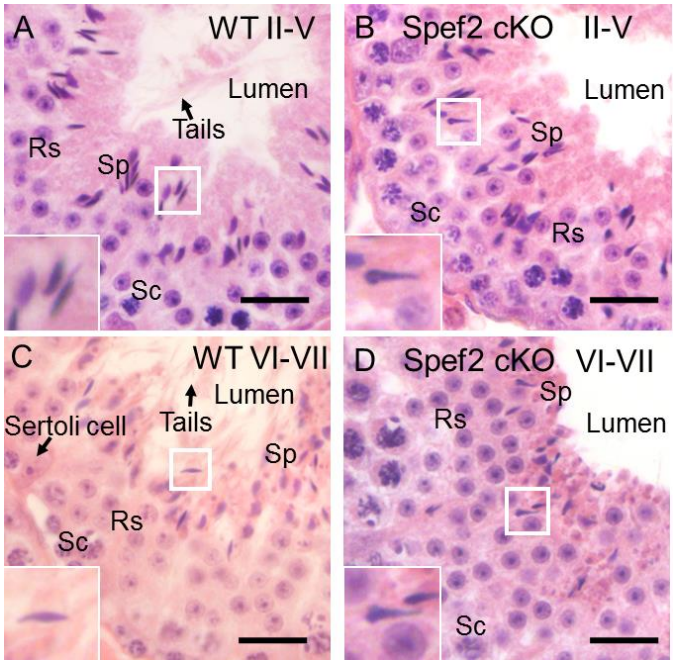

Figure 13. Loss of functional SPEF2 disrupts the head shaping and tail formation. HE stained WT and Spef2 cKO testis sections. Apart from several malformed sperm heads (B and D; marked with white squares and an insert) and the failure to form complete spermatid tails (B and D) the organisation of testis tubules in Spef2 cKO mice was similar to WT mice (A and C). The amount of step 15-16 spermatids appeared lower in Spef2 cKO (D) but the exact amount and onset of possible cell death was not assessed in more detail.The scale bar is 20µm. Sc=spermatocyte; Sp=spermatid; Rs=round spermatid

3.2.3 Loss of *Spef2* seems to have no apparent effect on acrosome biogenesis

After detecting the defective head shaping and the decrease in sperm count in HE staining the phenotype of Spef2 cKO mice was further characterized with fluorescence microscopy. To determine the reason behind abnormal head shape the acrosomes were stained with HPA that binds to Golgi derived acrosomal granule (Figure 14). WT

and Spef2 cKO step 2-7 round spermatids had identical looking dot-like acrosomes in HPA stainings (Figure 14 A-D) and the acrosome in step 14-16 elongating spermatids appeared to be unaffected by the loss of functional SPEF2 as the WT and Spef2 cKO acrosomes were seen to cover the other side of elongating spermatids (Figure 14 A-D). Moreover, no difference in acrosome biogenesis was observed between WT and Spef2 cKO testis sections in step 9-11 elongating spermatids (Figure 14 E and F). In conclusion, Spef2 cKO acrosomes seemed to be successfully formed and present throughout spermiogenesis in Spef2 cKO testis sections (Figure 14).

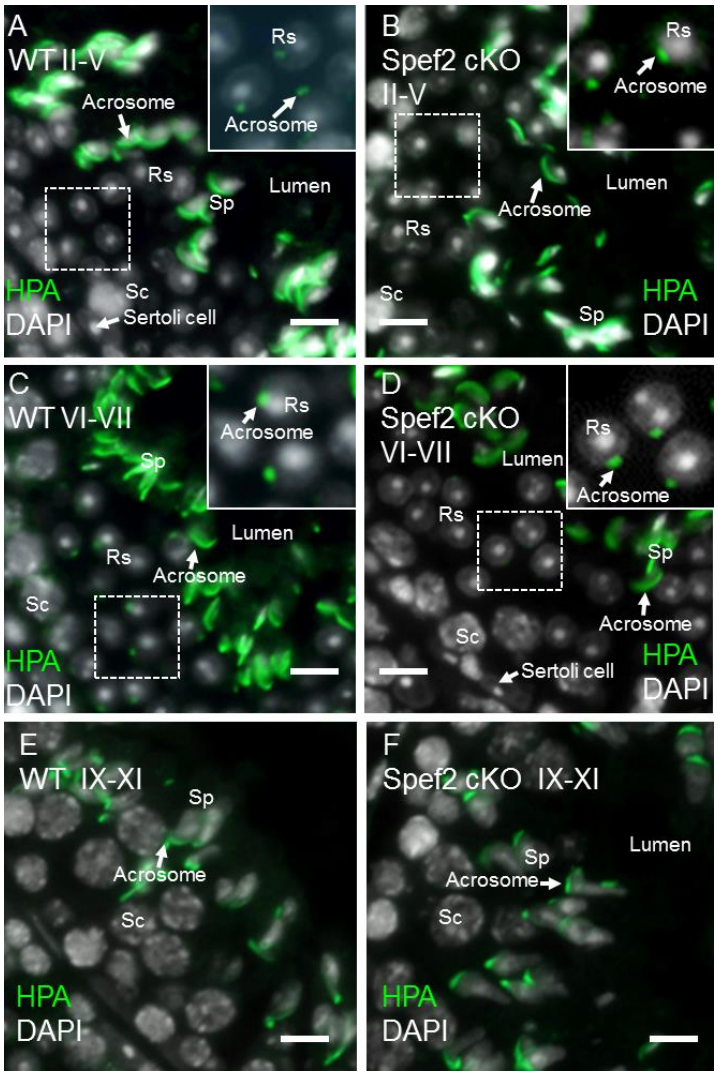

Figure 14. Loss of functional SPEF2 did not seem to affect the acrosome biogenesis in Spef2 cKO testis sections of stages II-VII and IX-XI. HPA was used to stain the acrosomal granule (in green) and DAPI (white) was used as a nuclear stain. (A and B) The acrosome in steps 2-5 round spermatids appeared to have formed identically between WT and Spef2 cKO testis sections (insert in A and B). Similarly, the acrosome of steps 14-15 spermatids in Spef2 cKO testis sections appeared to have normal morphology. (C and D) No acrosomal defects in step 6-7 round spermatids (inserts) and step 16 elongating spermatids were detected in Spef2 cKO testis sections. (E and F) No differences were detected between WT and Spef2 cKO step 9-11 acrosomes. The scale is 20 µm. Sc=spermatocyte; Sp=spermatid; Rs=round spermatid.

To confirm the HPA-results, the morphology and orientation of acrosome was additionally studied with PNA that binds to the whole acrosome (Figures 15 and 16). PNA supported the results gained from HPA staining showing no apparent defects in the morphology or orientation of acrosomes in Spef2 cKO mice.

3.2.4 In addition to acrosome biogenesis the apical ES seems to be unaffected in Spef2 cKO mice

The clear defects observed in spermiation of Spef2 cKO together with oddly-shaped sperm heads impelled for closer look on the relationship between Sertoli cell and spermatids. For this reason the apical ES between Sertoli cell and spermatids was investigated with actin-binding protein Espin. The apical ES appeared to form accordingly to cover the acrosome around step 7-8 round spermatids in both WT and Spef2 cKO (Figure 15 A and B). In the consequent steps 9-11 and 12-13 spermatids started to elongate and Sertoli cells were seen accordingly to increase the contact area of apical ES around the spermatids (Figure 15 C-F).

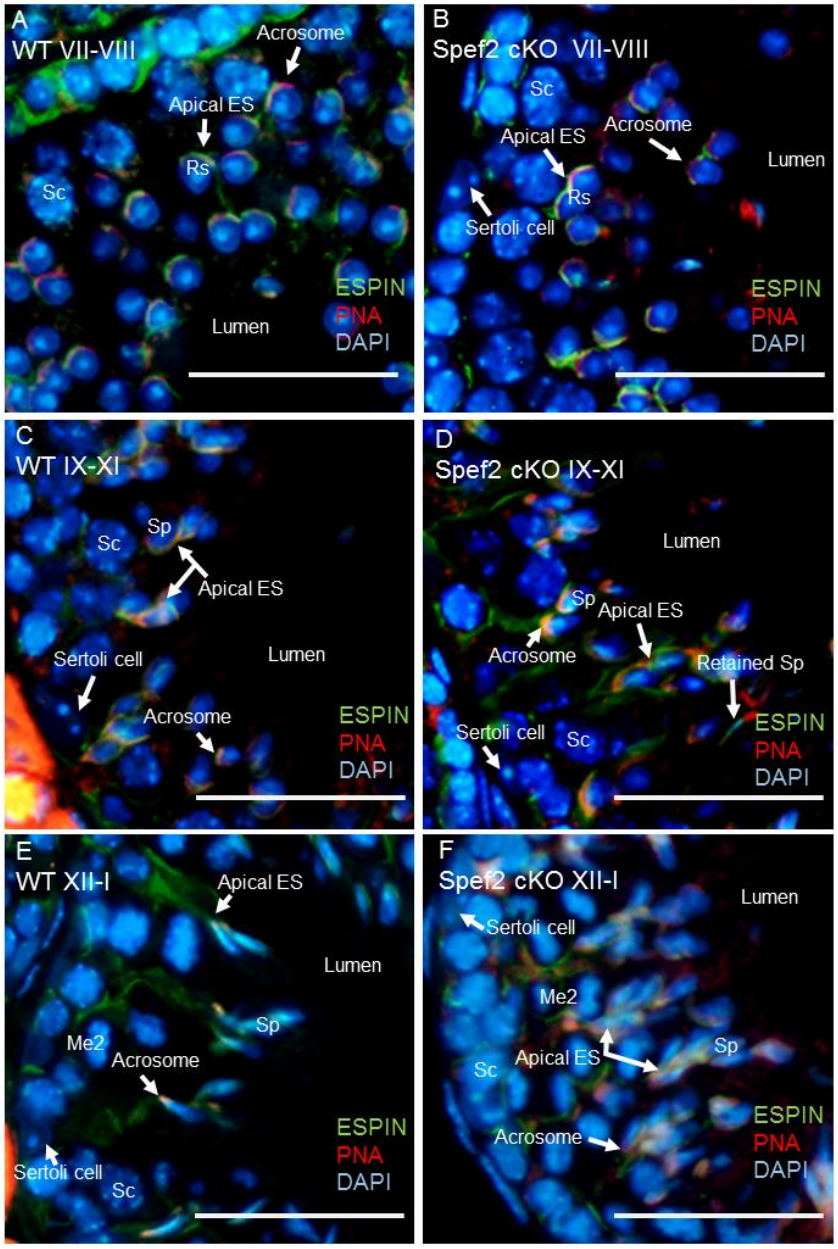

Figure 15. Acrosome biogenesis and apical ES during the stages VII-VIII, IX-XI and XII-I appeared similar between WT and Spef2 cKO mice. Espin antibody (green) was used to stain the apical ES, PNA (red) was used to stain the acrosomes and DAPI (blue) was used as a nuclear stain. (A and B) The apical ES was seen to form around steps 7-8 spermatids accordingly. Acrosome morphology was normal in Spef2 cKO steps 7-8 and 16 spermatids. (C and D) Apart from the retained sperm observed in Spef2 cKO section the acrosome biogenesis and apical ES during stages IX-XI seemed identical between WT and Spef2 cKO. (E and F) No difference in acrosome morphology of steps 12-13 spermatids or apical ES structures were observed in the stages XII-I. Meiosis 2 (Me2) seemed to occur normally. The scalebar is 20 μm.

Step 14-15 Spef2 cKO spermatids, similarly to WT spermatids, were seen to have been organized into bundle formation by Sertoli cells (Figure 16 A and B). In the WT and Spef2 cKO testis sections the apical ES was seen to surround step 16 spermatids prior to the spermiation in the stages VI-VII testis sections (Figure 16 C and D). In conclusion, the apical ES seemed identical between WT and Spef2 cKO throughout spermatogenesis (Figures 15 and 16).

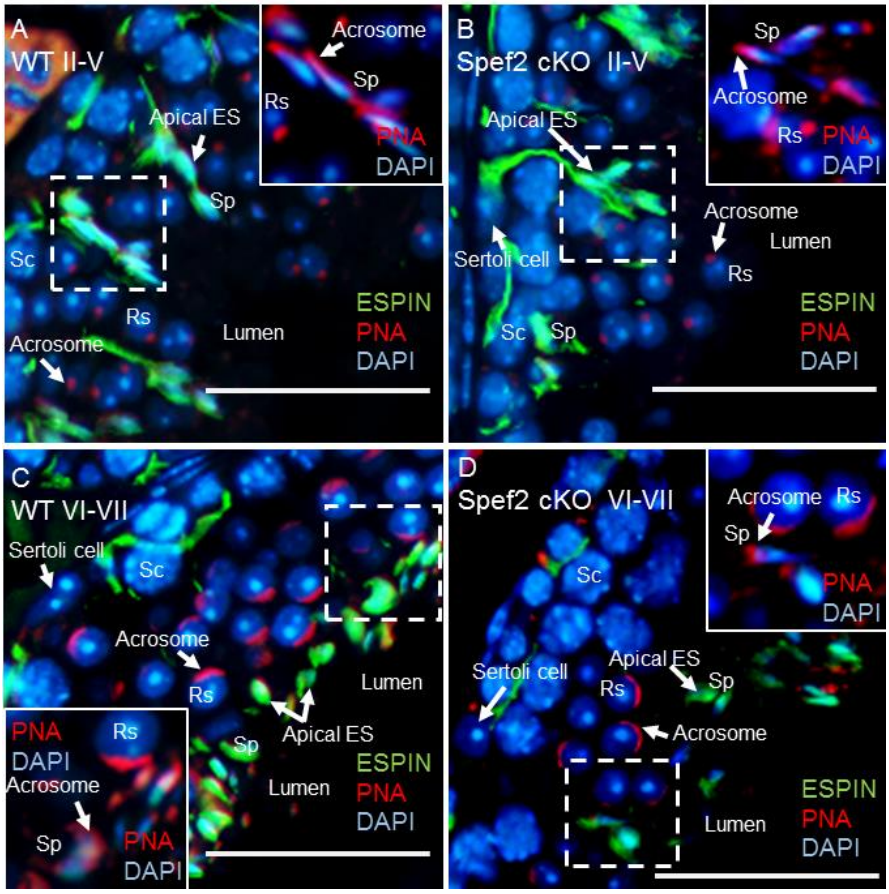

Figure 16. Testis sections from stages II-VII with acrosome staining (PNA; red) and apical ES staining (Espin antibody; green) showed identical progression of acrosome biogenesis and ES formation between WT and Spef2 cKO testis sections. The DAPI (blue) was used as a nuclear stain. (A and B) The spermatid bundle formation in which Sertoli cell are connected to the elongating spermatids (Sp) with the apical ES was observed to occur identically between WT and Spef2 cKO testis sections. The acrosome was unaffected by *Spef2* deletion in the steps 2-5 round spermatids (Rs). Likewise steps 14-15 spermatids had normal acrosomes (inserts in A and B). (C and D) Steps 16 elongated spermatids (Sp) were organized along the lumen by the Sertoli cells via apical ES accordingly. The steps 6-7 round spermatids and step 16 spermatids' acrosome were identical between WT and Spef2 cKO (inserts in C and D). The scalebar is 20 µm.

3.2.5 Non-functional SPEF2 results in the abnormal manchette and prevents sperm tail formation

The impaired manchette and tail formation in Spef2 cKO was further assessed due to the abnormally short or completely missing tails observed in HE-stainings of Spef2 cKO testis sections (Figure 12). The paraffin-embedded testis sections were stained with anti-acetylated alfa-tubulin antibody to determine the effect caused by the loss of functional SPEF2 on the manchette and tail formation (Figures 17 and 18). Supporting the results from the HE staining, the anti-acetylated alfa-tubulin staining of the Spef2 cKO mice testis sections showed that majority of sperm tails were either missing completely or appeared abnormally short compared to the WT counterparts (Figure 17).

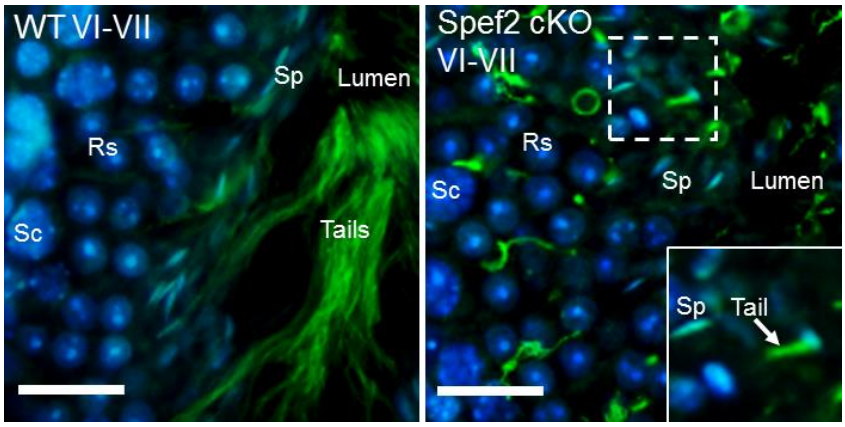

Figure 17. Spef2 cKO mice appeared to lack fully developed tails. The stage VI-VII testis section was stained with anti-acetylated alfa-tubulin (green) and DAPI (blue). Spef2 cKO testis section appeared to have stump tails (insert) or no tails at all whereas the lumen of WT testis section contained several tails. The scale is 20 µm.

Besides the stump tails (insert in Figure 17), abnormally long manchettes were observed in the Spef2 cKO steps 12-13 spermatids (insert in Figure 18 F). In contrast, the beginning of manchette formation in the steps 9-11 appeared to occur identically between WT and Spef2 cKO testis sections (Figure 18 A and B; C and D).

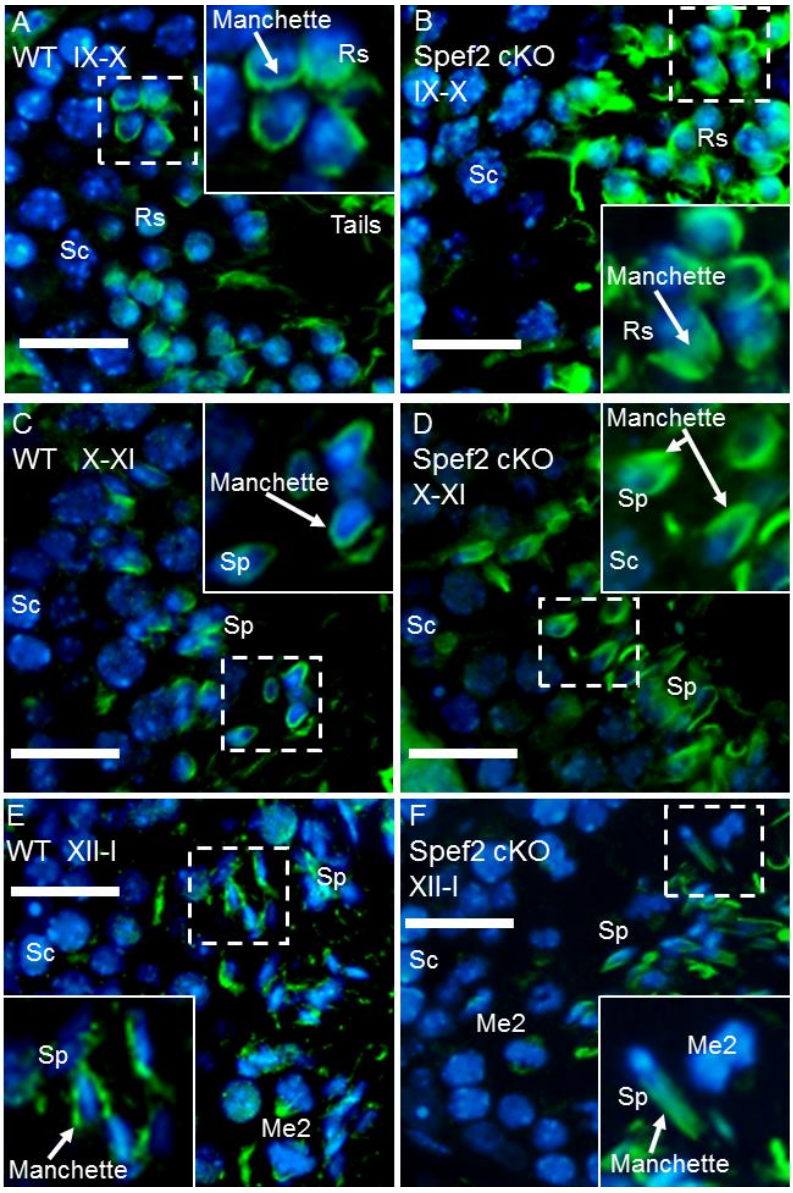

Figure 18. Manchette removal in the steps 12-13 spermatids was abnormal. Testis sections from stages IX-X, X-XI and XII-I stained with anti-acetylated alfa-tubulin antibody (green) and nuclear stain DAPI (blue). (A and B) The beginning of manchette formation in the steps 9-10 seemed identical between WT and Spef2 cKO (inserts of manchettes). (C and D) Similarly the *Spef2* deletion did not seem to affect the manchettes in steps 10-11 (inserts of manchettes). (E and F) In contrast to the previous steps, the manchettes in step 12-13 spermatids seemed abnormally long (an insert). Sc = spermatocyte; Rs = round spermatid; Sp = spermatid; Me2 = Meiosis 2. The scale is 20 µm.

In addition to the paraffin embedded testis sections, drying down samples stained with anti-alfa-tubulin antibody were used to investigate the abnormal manchette structure observed in the previous experiment. The shape of the manchette appeared normal in the steps 9-11 (Figure 19 A-D) but eventually seemed to grow abnormally long compared to the WT during steps 12-14 manchette (Figure 19 E and F).

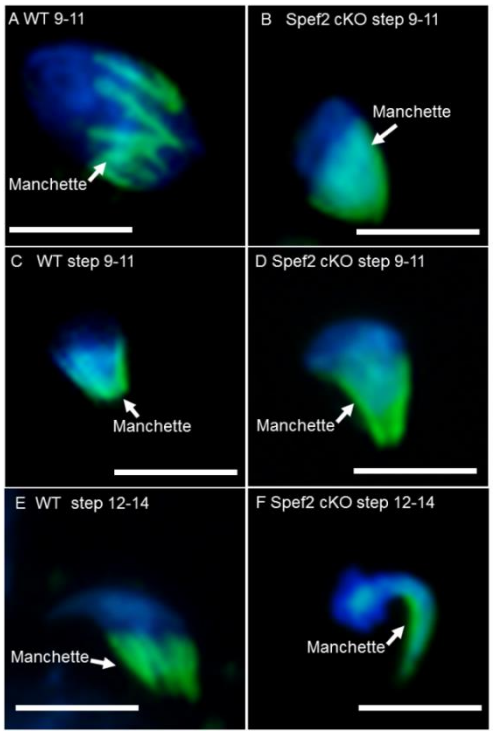

Figure 19. Spef2 cKO step 12 spermatids appeared to have abnormally long manchettes. Drying down samples stained with anti-alfa-tubulin antibody (green) and a nuclear stain DAPI (blue). (A-D) WT and Spef2 cKO manchettes appeared identical in the steps 9-11. (E and F) However, in the step 12-14 the manchette of Spef2 cKO was observed to have grown atypically long compared to its WT counterpart. The scale is 10 µm.

3.2.6 Depletion of *Spef2* appears to affect basal body formation

To further study the possible effects of *Spef2* deletion on tail assembly in Spef2 cKO mice basal bodies were stained with anti-gamma-tubulin antibody, a marker for the centrioles and basal bodies (Figures 20 and 21). Based on the identical looking gamma-tubulin signals in round spermatids of steps 2-7 (Figure 20) the loss of functional SPEF2 in Spef2 cKO mice did not appear to affect the basal bodies in the initiation phase of sperm tail formation. In contrast, Spef2 cKO steps 14-15 spermatids appeared to have enlarged basal bodies compared to the WT (Figure 20 B).

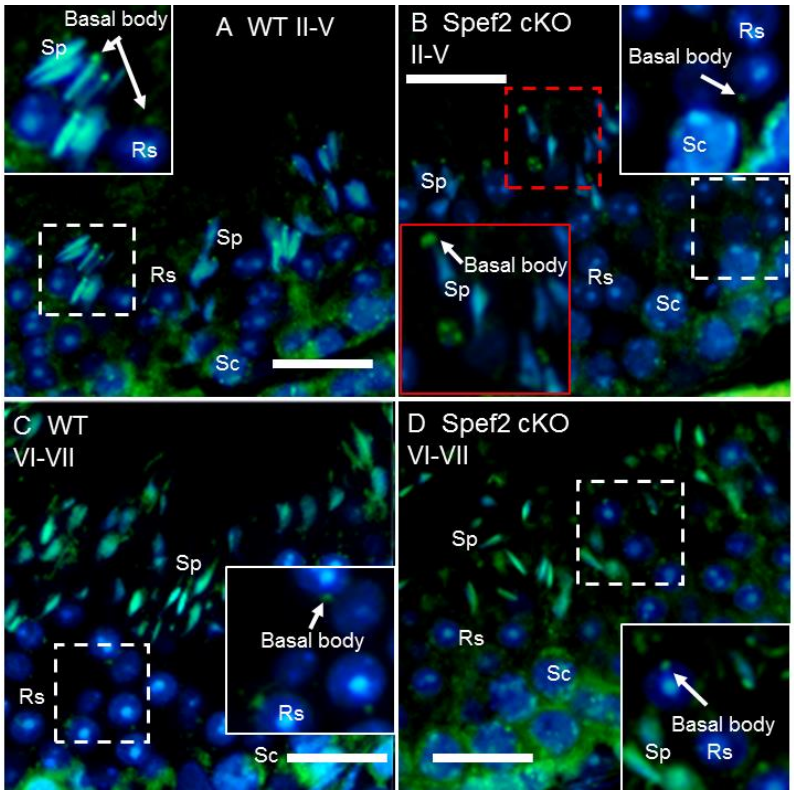

Figure 20. Loss of functional SPEF2 disorganizes basal bodies in late spermiogenesis. Spermatids were stained with anti-gamma-tubulin antibody (green) and nuclei with DAPI (blue). (A and B) In the Spef2 cKO testis section steps 14-15 spermatids appeared to have enlarged basal bodies (insert with red borders in B). In comparison the basal bodies in steps 2-5 round spermatids appeared similar to the WT (inserts in A and B (white borders)). (C and D) Steps 6-7 round spermatids continued to appear identical between WT and Spef2 cKO (inserts with white borders in C and D). The scalebar is 20 µm. Sc = spermatocyte; Rs = round spermatid, Sp = spermatid.

The malformation of the basal bodies in the Spef2 cKO mice was first detected the step 8-9 spermatids which showed multiple gamma-tubulin positive signals in the connecting piece (Figure 21 B). These signals retained during the later steps 9-15 (Figure 21 D and F). Similar staining was not observed in WT testis sections (Figure 21 A, C and E). In contrast, the centrosome duplication during meiosis 2 in the stage XII testis sections appeared to occur identically between WT and Spef2 cKO based on the two gamma-tubulin positive dots around a splitting secondary spermatocytes (insert in Figure 21 E and F (red borders)).

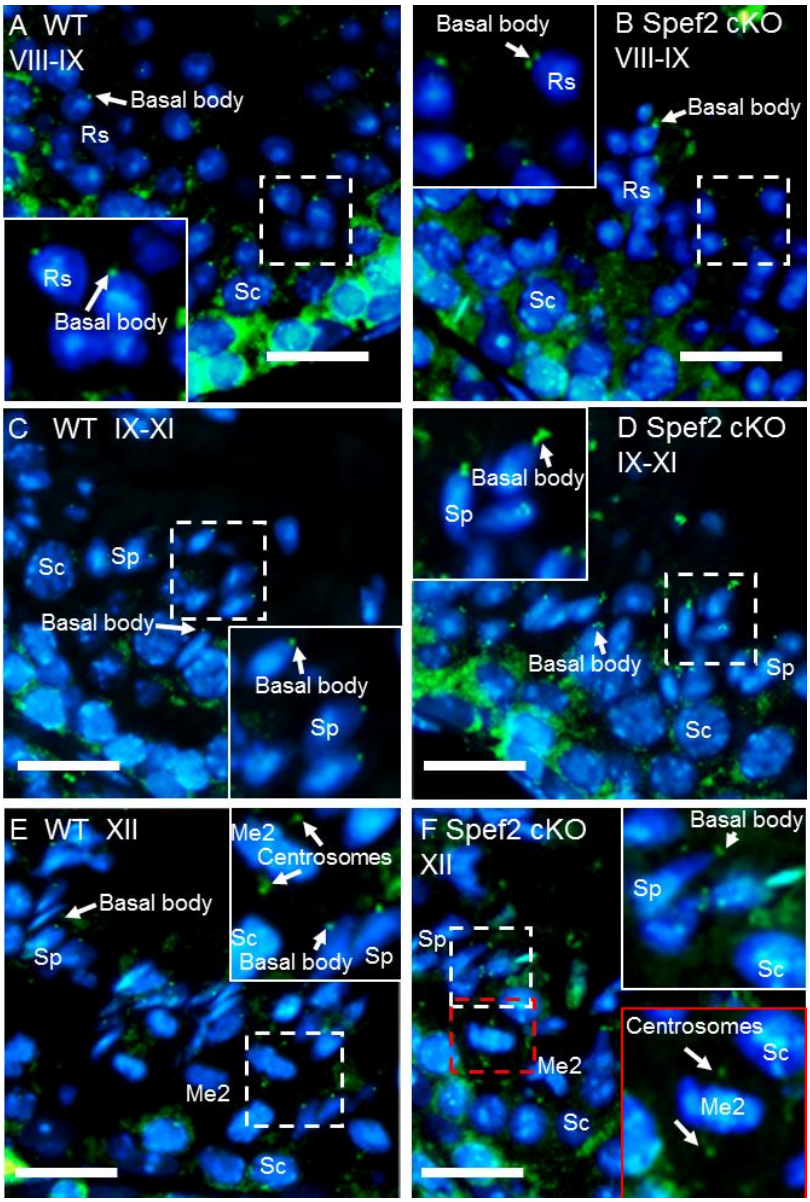

Figure 21. The malformed basal bodies in Spef2 cKO were first detected in step 8-9 spermatids. Basal bodies were stained with anti-gamma-tubulin antibody (green) and DAPI (blue) was used as a nuclear stain. (A and B) In contrast to WT testis section, the Spef2 cKO round spermatids seemed to have two gamma-tubulin signals in steps 8-9 (insert in B). (C and D) In the consequent steps 9-11 multiple gamma-tubulin signals in the place of one were observed in the Spef2 cKO testis section (insert in D). (E and F) During the stage XII meiosis 2 appeared to occur identically between WT and Spef2 cKO with an intact looking pair of centrosomes (inserts in E (white borders) and F (red borders)). However, the gamma-tubulin signal in step 12-13 spermatids seemed atypical. The scalebar is 20 µm. Sc = spermatocyte; Rs = round spermatid, Sp = spermatid, Me2 = meisosis 2.

Electron microscopy (EM) was utilized to confirm the origin of the multiple signals observed in gamma-tubulin-stained Spef2 cKO testis sections. The EM revealed a duplicated centrosome structure in Spef2 cKO testis sample (Figure 22).

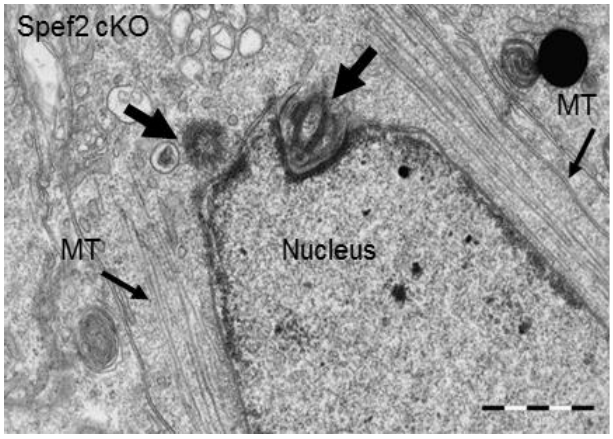

Figure 22. EM of Spef2 cKO male mouse's spermatid showed two centrosomal structures (thick arrows). MT denotes the microtubules of the manchette. The scalebar is 1 µm. The EM picture is modified from Mari Lehti's unpublished data.

3.3 Testing of novel anti-SPEF2 antibodies and localization of SPEF2 in elongating spermatids

Five anti-SPEF2 antibodies (Kad, KPL2end, GS-Spef2, Abnova, Sigma) with different binding sites within SPEF2 protein were tested in this study (Figure 23). Kad, GS-Spef2, Abnova and Sigma are novel antibodies with no previously published data, whereas, KPL2end has been previously tested on paraffin embedded testis sections, drying down samples and western blot by Sironen et al. (2010).

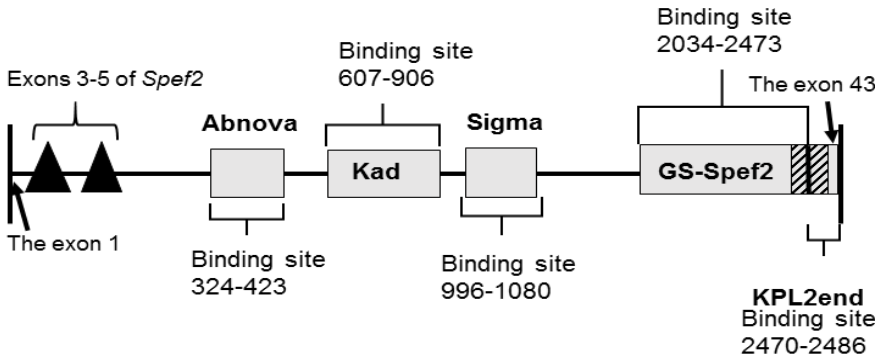

Figure 23. Schematic representation of the five anti-SPEF2 antibodies tested in this study and their designed binding sites within SPEF2 protein. The binding sites of the antibodies are located after the cleaved 3-5 exons of Spef2 cKO which is denoted here as a couple of black triangles. The overlapping area of binding sites of GS-Spef2 and KPL2end is represented with diagonal strokes. KPL2end was created to recognize a peptide corresponding to the exon 43 (Sironen et al. 2010).

Samples from Spef2 cKO mice were used as a control to verify specific binding of anti-SPEF2 antibodies in WT samples (Table 1). Since KPL2end was already reported not to work in paraffin embedded testis sections by Sironen et al. (2010) it was not re-tested in this study. Similarly to KPL2end, none of the novel anti-SPEF2 antibodies tested in this study, regardless of several optimization attempts, worked on the paraffin embedded cross-sections of the testis. Moreover, Abnova and Sigma anti-SPEF2 antibodies did not seem to work on cryo-sections either and were therefore excluded from the further experiments based on their poor performance. Kad, GS-Spef2 and KPL2end antibodies seemed to be suitable for cryo-section procedure, however the specific binding of Kad, KPL2end and GS-Spef2 needs to be verified with more staining optimization on testis cryo-sections before reporting any conclusive results. Kad was selected for further optimization in western blot and drying down samples.

Table 1. Testing results for five anti-SPEF2 antibodies. None of the anti-SPEF2 antibodies tested here was able to work with PFA-fixed testis sections. As Abnova and Sigma did not seem to work in neither pfa nor cryo-sections they were not used for further testing. GS-Spef2 seems to tentatively work in wb, dd and cryo but more optimization is needed. Kad antibody appears to work in cryo-sections, drying down preparations (dd) and western blot (wb). # = published by Sironen et al. (2010); * = more optimization needed to verify specific binding; long line = no specific binding detected.

Anti-SPEF2 antibody	Manufacturer	type	tested	works in
Kad	Abnova Lot#12048	Rabbit polyclonal	pfa (1:500-10.000), wb, dd cryo (1:1000 & 1:500)	wb (1:500), dd (1:500) cryo (1:500)*
KPL2end - raised against the exon 43 of *Spef2*	Abnova *Sironen et al. 2010*	Rabbit polyclonal	pfa#, wb#, dd#, cryo (1:500 & 1:250)	wb#, dd# cryo (1:250)*
GS-Spef2	GenScript	Rabbit polyclonal	pfa (1:500-1:5000), wb, dd cryo (1:1000 & 1:500)	wb (1:500)*, dd (1:500)* cryo (1:500)*
Abnova	Abnova H00079925-A01	Mouse polyclonal	pfa (1:250-2000) cryo (1:1000)	_____ _____
Sigma	Sigma HPA039606	Rabbit polyclonal	pfa (1:500) cryo (1:1000)	_____ _____

3.3.1 Kad antibody recognized the SPEF2 isoform 1 in the western blot

To this date there are estimated to be around 5-10 murine *Spef2* transcripts but only three of them (SPEF2 isoforms 1, 2 and 3; Table 2) have been verified. The binding site for Kad antibody is located at the region 607-906 aa within SPEF2 protein and this region is estimated to contain a potential ATP/GTP binding site (P-loop) in human SPEF2 (Table 2). This region is present in all SPEF2 products present in Ensembl database. Moreover, the *Spef2* transcripts, present in Ensembl, all contain 5' ends and are therefore potentially affected by the deletion of exons 3-5 in Spef2 cKO mice (Table 2). However, as the exact composition of exons in the majority of *Spef2* transcript is not known, they may not even contain the exons 3-5 and be transcribed regardless of the deletion of 3-5 exons in Spef2 cKO mice. According to previous research it seems that exon 4 is predominantly expressed in the testis and is absent in ciliated cells (Sironen et al. 2010). In addition to the splice variants lacking the deleted exons 3-5 from their 5' end, non-functional forms of *Spef2* transcripts may still be produced in Spef2 cKO mice.

Table 2. Five transcript isoforms (splice variants) of murine SPEF2 present in Ensembl database and the full-length SPEF2 isoform 1 from NCBI database. Only the isoforms 1, 2 and 3 (bolted text with grey background) have been verified. This table has only the estimated functional domains within each transcript present in Ensembl database. Table is modified from the *Spef2* transcript table by Ensembl (2015).

Murine *Spef2* transcripts	Transcript IDs	Exons	bp	aa	kDa	Domains
Spef2-001 Isoform 2	**ENSMUST00000041840 NP 796097.2**	**18**	**4247**	**875**	**100**	**CH, P-loop**
Spef2-002	ENSMUST00000160236	35	5313	1724	198	CH, P-loop
Spef2-003	ENSMUST00000159093	12	1917	622	73	P-loop
Spef2-006	ENSMUST00000162780	10	1639	513	61	P-loop
Spef2-004 Isoform 3	**ENSMUST00000159368 NP 001291973.1**	**9**	**1422**	**456**	**54**	**P-loop**
Isoform 1 full-length SPEF2	**NP 001291971.1**	**36**	**5565**	**1798**	**207**	**DUF1024 CH, ADK P-loop EF-hand**

The specificity of the Kad antibody was tested with western blot (Figure 24 A). Anti-α-tubulin was used as a control to verify equal protein concentrations between WT and Spef2 cKO samples (Figure 24 B). The Kad antibody recognized several bands that may correspond to possible shorter isoforms of SPEF2 or may be unspecific (Figure 24 A). However, Kad antibody recognized also circa 200 kDa band (arrows in Figure 24 A) in WT testis lysates that was not present in Spef2 cKO, and therefore most likely represent the SPEF2 isoform 1 (Figure 24 A).

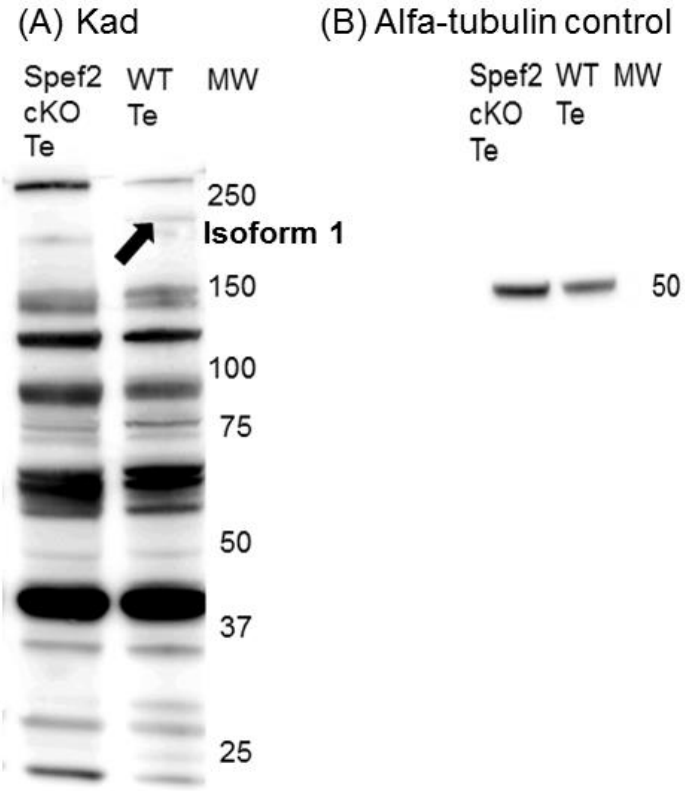

Figure 24. (A) Spef2 cKO and WT testis (Te) western blot with Kad antibody. SPEF2 isoform 1 (200 kDa, marked with an arrow) could be found in the WT testis lysate. (B) Anti-alfa-tubulin control was used to verify equal protein concentrations between WT and Spef2 cKO samples. Molecular weight (MW) is shown in kDa.

Some of the lower molecular weight bands (53 kDa, 60 kDa and 190 kDa) may correspond to estimated SPEF2 isoforms shown in Table 2. Overall, the abundance of protein bands expressed identically between WT and Spef2 cKO would strongly suggest that Kad antibody's binding ability to SPEF2 is not completely specific.

3.3.2 SPEF2 signal is detected from midpiece and basal body in drying down samples

In addition to western blot, Kad antibody seemed to bind SPEF2 in drying down samples (Figure 25). Kad signal was observed in the basal body and midpiece region of WT mouse elongated spermatids (Figure 25 A and C). Based on the lack of Kad-positive signal in Spef2 cKO samples (Figure 25 B and D) the basal body and midpiece signals appeared SPEF2-specific.

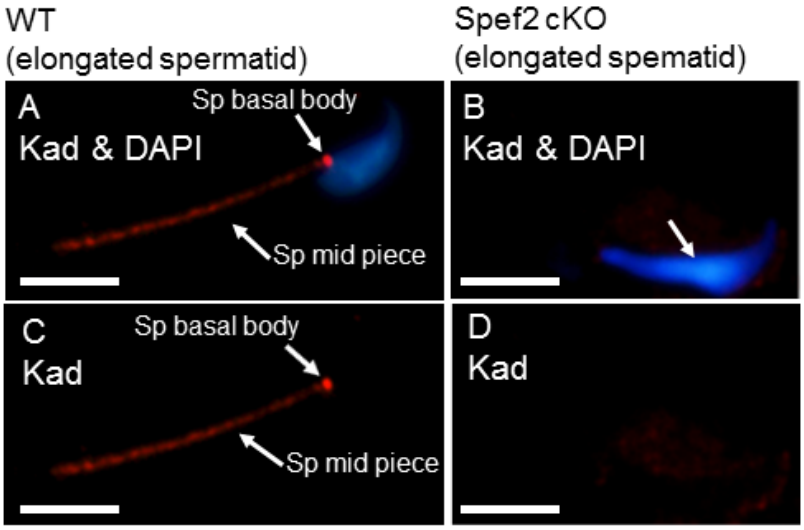

Figure 25. Kad was able to locate SPEF2 in elongated spermatid's basal body and midpiece of drying down samples (arrows in A and C). Kad (red) was tested as anti-SPEF2 antibody and DAPI (blue) was used in nuclear staining. Spef2 cKO drying down samples, used as a control, did not appear to have similar Kad staining (B and D). The scalebar is 10 µm. Sp = Spermatid.

4 Discussion

4.1 Loss of SPEF2 results in male infertility

In Spef2 cKO mice the cleaving of 3-5 exons of *Spef2* prevents the production of full length SPEF2 and renders the Spef2 cKO males effectively infertile. The defects in spermatogenesis of Spef2 cKO mice were validated by analyzing HE-stained cross-sections of the testis and epididymis of Spef2 cKO mice which revealed spermatids with truncated or missing tails and abnormally elongated sperm heads. Male infertility caused by perturbed SPEF2 function is consistent with the results of studies with ISTS (immotile short-tail sperm) pigs and bgh (big giant head) mice (Sironen et al. 2006, Sironen et al. 2011). Bgh mouse line suffers from sinusitis, severe hydrocephalus and male infertility caused by two single base substitution within *Spef2* (Sironen et al. 2011). The first nonsense mutation in exon 3 is assumed to result in nonfunctional protein domain and missense mutation in exon 28 is thought to result in a truncated protein product (Sironen et al. 2011). The impaired SPEF2 in bgh mice only affects the beating frequency of cilia but not the structural integrity whereas in sperm cells both the correct tail formation and function are compromised (Sironen et al. 2011). Since the full KO Spef2 mice (unpublished) and bgh mice (Sironen et al. 2011) often die prematurely Spef2 cKO mouse model was created in order to study the effect of *Spef2* deletion on spermatogenesis of adult male mice.

While the acrosome biogenesis seemed to be unaffected by *Spef2* deletion, further investigation into sperm-specific structures revealed an impaired manchette and basal body formation. In this study the acrosome biogenesis was shown for the first time to occur normally throughout the spermiogenesis in the absence of functional SPEF2. Interestingly, abnormal head shapes, development of the manchette and basal body has not been previously reported in either ISTS pigs or bgh mice (Andersson et al. 2000, Sironen et al. 2011). This phenotypical dissimilarity between previous animal models (Sironen et al. 2006, Sironen et al. 2011) and Spef2 cKO could be associated with the 5'-end of *Spef2* gene. In contrast to Spef2 cKO mouse model, ISTS pigs and bgh mice suffer from a deleterious mutation in the 3'-end which does not prevent the expression of 5'-end *Spef2* transcripts.

4.1.1 *Spef2* deletion affects sperm production and spermiation

In addition to defects in spermatid morphology, deletion of *Spef2* appeared to result in disrupted spermiation and reduction in the number of elongating spermatids in Spef2 cKO mice. The most dramatic difference in the spermatid count between WT and Spef2 cKO mice seemed to occur during the steps 15 and 16. Therefore, the scarce amount of sperm cells in epididymis of Spef2 cKO mice seems to be caused by the dramatic depletion in spermatid numbers during the spermiogenesis as well as the spermiation failure. Presence of spermatozoa albeit in extremely few numbers in epididymis indicates that the spermiation was not completely defective. However, since TUNEL assay and quantitative assessment of spermatids during each stage were not carried out it is difficult to pinpoint the exact onset of cell death in Spef2 cKO spermiogenesis as well as the exact number of spermatids. The significantly low number of spermatozoa in epididymis has also been reported to occur in ISTS affected pigs and bgh mice (Andersson et al. 2000, Sironen et al. 2011). Spermiation failure is a typical symptom in genetically-modified mouse models with defective spermatogenesis (O'Donnell et al. 2011). Therefore, the spermiation failure observed in this study is most probably an indirect result from the abnormal morphology of Spef2 cKO spermatids.

4.1.2 Abnormal manchette elongation results in impaired spermatid head shaping in Spef2 cKO

In Spef2 cKO mice the appearance of impaired manchette was simultaneous with the emergence of abnormal club-shaped sperm heads. Therefore, the defective manchette elongation is implicated as the main cause for the impaired sperm head shaping in Spef2 cKO mice. Based on this SPEF2 appears to have an important role in manchette development and regulation. This hypothesis is further supported by a previous study which showed that SPEF2 localizes in the manchette (Sironen et al. 2010). In contrast to Spef2 cKO club-shaped spermatids, round headed sperm morphology is commonly associated with acrosome defects (Kierszenbaum et al. 2004). The unaffected acrosome biogenesis in Spef2 cKO mice indicates that the abnormal head shape caused by *Spef2* deletion is mediated independently from acrosome formation.

4.1.3 SPEF2 may be a non-structural component of manchette

Spef2 cKO mice do not exhibit the disorganized microtubule structure or detachable manchette phenotype observed in azh, Sun4, E-Map-115 and Clip-170 mutant mice (Meistrich et al. 1990, Komada et al. 2000, Akhmanova et al. 2005, Calvi et al. 2015). Based on these phenotypic differences, it is unlikely that SPEF2 would function as a structural linking protein between microtubules and nuclear envelope or be involved in

organizing the microtubules within manchette. Moreover, unlike microtubule-associated proteins (MAPs) SPEF2 does not seem to have a microtubule binding domain. Therefore, SPEF2 may be involved in manchette removal or in cargo transportation, which could be achieved in interaction with other proteins such as its known interacting partner IFT20 (Sironen et al. 2010). In comparison, SPEF2 does have a potential actin-binding domain. Therefore, SPEF2 might function as an actin binding site within manchette. However, as the actin binding potential of SPEF2 is yet to be confirmed, it is not certain whether the actin binding ability has any real relevance to SPEF2's role in the manchette.

4.1.4 SPEF2 may regulate the manchette removal via IMT

In previous study by Sironen et al. (2010) IFT20 was shown to be co-localized with SPEF2 in the spermatid manchette. Based on the SPEF2 protein's association with IFT20, the potential disruption of IMT in Spef2 cKO mice is likely to be mediated via a microtubule pathway rather than F-actin tracks. Interestingly, the tail formation together with the sperm head shaping is defective in the germ cell specific KIF3A cKO mouse model (Lehti et al. 2013). Similarly to Spef2 cKO, KIF3A cKO mice (Lehti et al. 2013) express the club-like spermatid head phenotype and similarly elongated manchette. In KIF3A cKO mice the abnormal manchette phenotype was assumed to result from the defective manchette clearance (Lehti et al. 2013). Based on the phenotypic similarities between Spef2 cKO and KIF3A cKO, it seems likely that the testis-specific isoform of SPEF2, similarly to KIF3A, is involved in manchette clearance.

4.1.5 Deletion of *Spef2* causes truncated sperm tails in Spef2 cKO mice

Consistent with the bgh mice (Sironen et al. 2011) the Spef2 cKO mice seem to lack fully developed sperm tails. The presence of basal bodies and occasional stump tails in Spef2 cKO indicate that formation of the sperm tail was initiated but failed to proceed normally. Failure to complete sperm tail is a common fate observed among mice with defective IFT such as ORPK (Oak Ridge Polycystic Kidney) mice (Lehman et al. 2008). IFT is responsible for the axoneme formation and cargo transport in cilia and sperm tails (Ishikawa & Marshall 2011). In ORPK mice the hypomorphic mutation of *ift88* gene disrupts ciliogenesis and sperm tail formation by rendering the IFT dysfunctional (Lehman et al. 2008, Kierszenbaum et al. 2011b). IFT88 and IFT20 are components of IFT complex B that participates in the anterograde IFT (Ishikawa & Marshall 2011). Therefore, it is within reason to speculate that SPEF2 as an interacting partner for IFT20 may be either part of the IFT complex B or somehow closely involved in the IFT complex B related activities.

However, while both bgh mice and ISTS pigs are shown to have impaired sperm tail formation, in somatic cells neither appears to have ultrastructural defects nor affected ciliogenesis (Andersson et al. 2000, Sironen et al. 2011). This would indicate that in somatic cells the IFT complex B is functional without the presence of SPEF2. Therefore, whether the impaired sperm tail development in Spef2 cKO is truly caused by defective IFT complex B requires more research. It is possible that ciliated cells and sperm cells might have a slightly different combination of proteins associated with the IFT complex B and as a consequence SPEF2 is only essential in sperm tail formation. In addition, SPEF2 has various tissue-specific isoforms among which the full length 200 kDa isoform is testis specific. Therefore, it is likely that SPEF2 has isoform and tissue-specific roles in animal cells. This seems to apply to bgh mice in which SPEF2 was suggested to regulate the beat frequency but not ciliogenesis (Sironen et al. 2011). In ciliated cells SPEF2 has been proposed to be associated with the central pair instead (Sironen et al. 2011). Furthermore, while SPEF2 may be merely cargo shuttled by IFT complex B, the truncated tail phenotype is similar to mice models with perturbed IFT caused by a defective key factor in IFT such as that of KIF3A cKO mice (Lehti et al. 2013). Therefore, it would be tempting to speculate that SPEF2 would directly participate in IFT or its regulation.

In a recent study by San Augustin et al. (2015) several IFT complex B (IFT88, IFT57 and IFT20) and IFT complex A (IFT140) proteins were reported to be absent in mature murine sperm tails which lead the authors to speculate an arrest of IFT after sperm cell maturation. In contrast, SPEF2 is known to persist in the distal part of the murine sperm tail midpiece (Sironen et al. 2010). This would suggest a structural role in the sperm tail. Similarly to SPEF2, KIF3A appears to remain in the mature sperm (Lehti et al. 2013). Additional work is needed to confirm whether SPEF2 is a component of IFT complex B, its cargo, such as a structural protein of the sperm tail, or an IFT regulatory protein.

4.1.6 Loss of functional SPEF2 may affect the basal bodies

Based on the basal body duplication observed in immunofluorescent stainings and EM, SPEF2 may be involved in basal body regulation. Kierszenbaum (2002a) has suggested that IMT could be responsible for the transport of the building blocks needed in the centrosome. Therefore, the disturbed basal body structure seen in Spef2 cKO mice could be caused by defective IMT and/or IFT. Consistent with the putative role of IFT in basal body regulation, the auditory hair cell specific KIF3A cKO mouse model was shown to have defective positioning of basal bodies (Sipe & Lu 2011). In turn the

deletion of *ift88* has been shown to cause defective migration of basal bodies in auditory hair cells (Jones et al. 2008). Both studies demonstrated a clear connection between IFT particles and basal body regulation albeit only in somatic cells. Kierszenbaum et al. (2011b) additionally reported a duplicated axoneme in ift88 mutant mice. In the germ cell specific KIF3A cKO mouse model KIF3A has been shown to localize in basal bodies but rather surprisingly the deletion of *Kif3a* seemed to have no effect on the position or structure of the spermatids' basal bodies (Lehti et al. 2013).

Similarly to KIF3A, SPEF2 was found to localize in the basal body region of spermatids when stained with Kad and in a previous study with the KPL2end antibody (Sironen et al. 2010). Interestingly, the loss of full length SPEF2 did not seem to result in structural defects in cilia nor basal bodies of bgh mice (Sironen et al. 2011). Therefore, it seems that a shorter 5' end isoform of SPEF2 may contribute to the basal body regulation specifically during the later steps of spermiogenesis. The regulation of the basal body seems to vary between ciliated cells and sperm cells as demonstrated by KIF3A mouse models (Sipe & Lu 2011, Lehti et al. 2013, Liu et al. 2015). This might explain why the somatic cells in Spef2 KO mice do not exhibit any basal body irregularities. To confirm whether the underlying cause for malformed basal bodies in Spef2 cKO mice is impaired IMT and/or IFT, needs more extensive research. Alternatively, SPEF2 might also affect the basal body directly as a structural protein or regulate other proteins involved in basal body regulation. Moreover, the duplication of the basal body observed in Spef2 cKO mice could be an indirect result from the overall failure of spermiogenesis.

4.2 Kad seems to be able to detect the SPEF2 isoform 1 in western blot and drying down samples

In Spef2 cKO mice the deletion of exons 3-5 results in a non-functional form of SPEF2 isoform 1 of circa 170 kDa (unpublished data). Therefore, Spef2 cKO may contain other non-functional forms of shorter *Spef2* transcripts as well. However, based on the western blot results, Kad was not able to recognize the non-functional form of SPEF2 isoform 1 and seems to be able to bind SPEF2-specifically. Similarly to the western blot with KPL2end by Sironen et al. (2010) several other bands, apart from the full-length SPEF2 isoform 1, were detected in the Kad western blot. While some of the bands might represent additional *Spef2* transcripts, they may also be simply degradation products or a result of unspecific binding. Moreover, Spef2 cKO mouse model is likely to contain non-functional forms of transcripts and consequently their degradation products. The relatively large quantity of bands between WT and Spef2 cKO observed in the Kad western blot tends to point to unspecific binding. Conversely, some of the

identical bands between WT and Spef2 cKO might also be due to the transcripts that do not contain the exons 3-5 and are therefore unaffected by the cleaving of exons in Spef2 cKO mice. Verification of potential *Spef2* transcripts in the Kad western blot would require mass spectrometry analysis. To this date only three murine isoforms of SPEF2 have been verified while around 10 transcripts in total have been estimated to exist (NCBI). More murine *Spef2* transcripts are likely to arise in the future. Identification of *Spef2* transcripts would help with understanding the diverse roles of different SPEF2 transcripts in ciliogenesis and spermatogenesis.

In addition to recognizing the SPEF2 isoform 1 in the western blot, Kad was able to localize SPEF2 in the spermatid tail midpiece and basal body. This is consistent with the results of the KPL2end staining by Sironen et al. (2010). KPL2end has been additionally found to stain the Golgi complex of spermatocytes and round spermatids (Sironen et al. 2010). Similarly to KPL2end, Kad is also seen to localize in the Golgi in this study. However, unlike the basal body and midpiece stainings, the Golgi staining was also observed in Spef2 cKO samples. Thus, more testing is needed to verify whether the Golgi signal observed in the spermatocytes of Spef2 cKO and WT mice is a sign of Golgi-specific isoform of SPEF2.

4.3 Future studies

Overall, the findings from the Spef2 cKO mouse model highlight the importance of studying the axoneme and manchette formation in mammalian spermatogenesis. Albeit cilium and sperm tail assembly are very similar and advances in both fields is mutually beneficial, mammalian sperm tail structure development has its own characteristics not found in studies of ciliated cells. One of these unique characteristics of spermatogenesis is the formation of the manchette and IMT that seem to regulate the head shaping in spermatids and sperm tail elongation (Kierszenbaum & Tres 2004). Although this study provides new insight into the function of SPEF2 in spermatogenesis, additional experiments are needed to completely characterize the Spef2 cKO phenotype and assess the exact role of SPEF2 in spermatid and sperm tail development. Particularly, the sperm tail assembly in Spef2 cKO could be further examined since this study did not include in detail investigation of the disorganization level of Spef2 cKO sperm tail. Therefore, it would be interesting to study the axoneme and the accessory tail structures of Spef2 cKO with EM. In addition to EM, phase contrast microscopy is a standard procedure to study the morphology of the sperm tail as well as acrosome formation. Similarly, sperm head structures such as basal body and manchette formation could be examined in greater detail with EM.

The assembly and disassembly of apical ES and tubulobulbar complexes (TBC) could be studied in greater detail with EM before ruling out a possible defect in them causing the spermiation failure observed in Spef2 cKO mice. As the deletion of the full-length isoform of SPEF2 is strictly germ cell specific in this mouse model, Sertoli cells are not directly affected by the deletion. Therefore, a more effective method of studying the effect of *Spef2* deletion on Sertoli cell germ cell interaction would be using a mouse model in which the Sertoli cells as well would be lacking the SPEF2 protein. Additionally, a mouse model with GFP-tagged-SPEF2 could show the localization pattern of SPEF2 more reliably. Furthermore, it could be used to visualize whether SPEF2 is a mobile or static component within the manchette and sperm tail. Acrosome biogenesis was confirmed to proceed normally in the absence of full-length SPEF2 in this study but the condition of acroplaxome was not yet assessed.

To verify the credibility of novel antibodies, they need to be able to function on various sample methods. Moreover, different preparations of tissue show different histological aspects. Paraffin-embedded and cryo-sections can show overall organization of seminiferous tubules and cytoplasmic staining, while drying down and squash preparations allow studies of the condition of individual cells and the exact localization of a target protein in cell structures in more detail. In this study Kad was shown to work when using drying down samples and western blot but the protocol for immunofluorescence in cryo-sections needs to be optimized further. Similarly, GS-Spef2 antibody may have potential to work after additional protocol optimization on western blot, drying down samples and cryo-sections. Information on interaction partners could help elucidate the exact mechanism behind the Spef2 cKO male infertility. Thus far, only one interaction partner (IFT20) has been discovered (Sironen et al. 2010). Therefore, co-immunoprecipitation (Co-IP) could be carried out to detect potential interaction partners from WT testis lysates using the novel anti-SPEF2 antibodies such as Kad. Possible candidates derived from Co-IP could then be identified with mass spectrometric analysis.

5 Acknowledgements

This study was carried out in Department of Physiology, Institute of Biomedicine, University of Turku. The material and reagents for the thesis were provided by former MTT (Agrifood Research Finland) and Department of Physiology, Institute of Biomedicine, University of Turku. I would first like to thank my thesis supervisors: Principal scientist Anu Sironen and PhD student Mari Lehti from MTT (after fusion with other Research institutes in Finland currently called Luke; Natural Resources Institute Finland). In addition, I would like to express gratitude to my thesis advisor, Assistant Professor Noora Kotaja, from Department of Physiology Institute of Biomedicine University of Turku. I am gratefully indebted to their guidance in both the experiments for thesis and thesis writing. This accomplishment would not have been possible without their expertise. I would also like to acknowledge my additional thesis advisor, Tiina Henttinen, from Division of Genetics and Physiology, Department of Biology, University of Turku. I am profoundly grateful for her valuable encouragement and comments on this thesis. I would additionally like to thank the staff of Department of Physiology, Institute of Biomedicine, University of Turku for advices and help in the experiments for my thesis. Similarly, I would like to express my gratitude to Johanna Rusi and Tarja Hovivuori in MTT for PCR work. Finally, I would like to express thanks to my family and friends for emotional support and encouragement during the whole process.

6 References

Akhmanova A, Mausset-Bonnefont AL, van Cappellen W, Keijzer N, Hoogenraad CC, Stepanova T, Drabek K, van der Wees J, Mommaas M, Onderwater J, van der Meulen H, Tanenbaum ME, Medema RH, Hoogerbrugge J, Vreeburg J, Uringa EJ, Grootegoed JA, Grosveld F & Galjart N. 2005. The microtubule plus-end-tracking protein CLIP-170 associates with the spermatid manchette and is essential for spermatogenesis. *Genes & Development* 19 (20), 2501-2515.

Andersson M, Peltoniemi O, Makinen A, Sukura A & Rodriguez- Martinez H. 2000. The Hereditary 'Short Tail'Sperm Defect- A New Reproductive Problem in Yorkshire Boars. *Reproduction in Domestic Animals* 35 (2), 59-63.

Barratt CL, Mansell S, Beaton C, Tardif S & Oxenham SK. 2011. Diagnostic tools in male infertility-the question of sperm dysfunction. *Asian Journal of Andrology* 13 (1), 53-58.

Bartles JR, Wierda A & Zheng L. 1996. Identification and characterization of espin, an actin-binding protein localized to the F-actin-rich junctional plaques of Sertoli cell ectoplasmic specializations. *Journal of Cell Science* 109 (Pt 6) (Pt 6), 1229-1239.

Beever DE. 2006. The impact of controlled nutrition during the dry period on dairy cow health, fertility and performance. *Animal Reproduction Science* 96 (3-4), 212-226.

Berruti G & Paiardi C. 2014. The dynamic of the apical ectoplasmic specialization between spermatids and Sertoli cells: the case of the small GTPase Rap1. *BioMed Research International* 2014, 635979.

Boivin J, Bunting L, Collins JA & Nygren KG. 2007. International estimates of infertility prevalence and treatment-seeking: potential need and demand for infertility medical care. *Human Reproduction (Oxford, England)* 22 (6), 1506-1512.

Borg CL, Wolski KM, Gibbs GM & O'Bryan MK. 2010. Phenotyping male infertility in the mouse: how to get the most out of a 'non-performer'. *Human Reproduction Update* 16 (2), 205-224.

Brandes M, Hamilton CJ, de Bruin JP, Nelen WL & Kremer JA. 2010. The relative contribution of IVF to the total ongoing pregnancy rate in a subfertile cohort. *Human Reproduction (Oxford, England)* 25 (1), 118-126.

Brandes M, Hamilton CJ, van der Steen JO, de Bruin JP, Bots RS, Nelen WL & Kremer JA. 2011. Unexplained infertility: overall ongoing pregnancy rate and mode of conception. *Human Reproduction (Oxford, England)* 26 (2), 360-368.

Buffone MG, Foster JA & Gerton GL. 2008. The role of the acrosomal matrix in fertilization. *The International Journal of Developmental Biology* 52 (5-6), 511-522.

Calvi A, Wong AS, Wright G, Wong ES, Loo TH, Stewart CL & Burke B. 2015. SUN4 is essential for nuclear remodeling during mammalian spermiogenesis. *Developmental Biology* .

Cardenas-Rodriguez M & Badano JL. 2009. Ciliary biology: understanding the cellular and genetic basis of human ciliopathies. *American Journal of Medical Genetics.Part C, Seminars in Medical Genetics* 151C (4), 263-280.

Clermont Y, Morales C & Hermo L. 1987. Endocytic activities of Sertoli cells in the rat. *Annals of the New York Academy of Sciences* 513, 1-15.

Cohen PE, Pollack SE & Pollard JW. 2006. Genetic analysis of chromosome pairing, recombination, and cell cycle control during first meiotic prophase in mammals. *Endocrine Reviews* 27 (4), 398-426.

Ensembl.2015.*Spef2.<http://www.ensembl.org/Mus_musculus/Gene/Summary?db=core;g=ENSMUSG00000072663;r=15:9578193-9748868 > [Accessed 14.2.2016]*

Finn R, Evans CC & Lee L. 2014. Strain-dependent brain defects in mouse models of primary ciliary dyskinesia with mutations in Pcdp1 and Spef2. *Neuroscience* 277, 552-567.

Flowers WL. 2013. Triennial Reproduction Symposium: sperm characteristics that limit success of fertilization. *Journal of Animal Science* 91 (7), 3022-3029.

Goto M, O'Brien DA & Eddy EM. 2010. Speriolin is a novel human and mouse sperm centrosome protein. *Human Reproduction (Oxford, England)* 25 (8), 1884-1894.

Hermo L, Pelletier R-, Cyr DC & Smith CE. 2010a. Surfing the Wave, Cycle, Life History, and Genes/Proteins Expressed by Testicular Germ Cells. Part 1: Background to Spermatogenesis, Spermatogonia, and Spermatocytes. *Microscopy Research and Technique* 73 (4), 243-278.

Hermo L, Pelletier R-, Cyr DG & Smith CE. 2010b. Surfing the Wave, Cycle, Life History, and Genes/Proteins Expressed by Testicular Germ Cells. Part 2: Changes in Spermatid Organelles Associated With Development of Spermatozoa. *Microscopy Research and Technique* 73 (4), 279-319.

Hess RA & de Franca LR. 2008. Spermatogenesis and cycle of the seminiferous epithelium. *Molecular mechanisms in spermatogenesis.* Springer. 1-15.

Ho HC & Wey S. 2007. Three dimensional rendering of the mitochondrial sheath morphogenesis during mouse spermiogenesis. *Microscopy Research and Technique* 70 (8), 719-723.

Horowitz E, Zhang Z, Jones BH, Moss SB, Ho C, Wood JR, Wang X, Sammel MD & Strauss JF,3rd. 2005. Patterns of expression of sperm flagellar genes: early expression of genes encoding axonemal proteins during the spermatogenic cycle and shared features of promoters of genes encoding central apparatus proteins. *Molecular Human Reproduction* 11 (4), 307-317.

Hu Y, Yu H, Pask AJ, O'Brien DA, Shaw G & Renfree MB. 2009. A-kinase anchoring protein 4 has a conserved role in mammalian spermatogenesis. *Reproduction (Cambridge, England)* 137 (4), 645-653.

Huckins C. 1971a. The spermatogonial stem cell population in adult rats. 3. Evidence for a long-cycling population. *Cell and Tissue Kinetics* 4 (4), 335-349.

Huckins C. 1971b. The spermatogonial stem cell population in adult rats. I. Their morphology, proliferation and maturation. *The Anatomical Record* 169 (3), 533-557.

Huckins C. 1971c. The spermatogonial stem cell population in adult rats. II. A radioautographic analysis of their cell cycle properties. *Cell and Tissue Kinetics* 4 (4), 313-334.

Hull MG, Glazener CM, Kelly NJ, Conway DI, Foster PA, Hinton RA, Coulson C, Lambert PA, Watt EM & Desai KM. 1985. Population study of causes, treatment, and outcome of infertility. *British Medical Journal (Clinical Research Ed.)* 291 (6510), 1693-1697.

Ibanez-Tallon I, Heintz N & Omran H. 2003. To beat or not to beat: roles of cilia in development and disease. *Human Molecular Genetics* 12 Spec No 1, R27-35.

Irvine DS. 1998. Epidemiology and aetiology of male infertility. *Human Reproduction* 13 (suppl 1), 33-44.

Ishikawa H & Marshall WF. 2011. Ciliogenesis: building the cell's antenna. *Nature Reviews.Molecular Cell Biology* 12 (4), 222-234.

Jones C, Roper VC, Foucher I, Qian D, Banizs B, Petit C, Yoder BK & Chen P. 2008. Ciliary proteins link basal body polarization to planar cell polarity regulation. *Nature Genetics* 40 (1), 69-77.

Kierszenbaum AL. 2002a. Intramanchette transport (IMT): managing the making of the spermatid head, centrosome, and tail. *Molecular Reproduction and Development* 63 (1), 1-4.

Kierszenbaum AL. 2002b. Sperm axoneme: a tale of tubulin posttranslation diversity. *Molecular Reproduction and Development* 62 (1), 1-3.

Kierszenbaum AL. 2001. Spermatid manchette: plugging proteins to zero into the sperm tail. *Molecular Reproduction and Development* 59 (4), 347-349.

Kierszenbaum AL, Rivkin E & Tres LL. 2007. Molecular biology of sperm head shaping. *Society of Reproduction and Fertility Supplement* 65, 33-43.

Kierszenbaum AL, Rivkin E & Tres LL. 2003. Acroplaxome, an F-actin-keratin-containing plate, anchors the acrosome to the nucleus during shaping of the spermatid head. *Molecular Biology of the Cell* 14 (11), 4628-4640.

Kierszenbaum AL, Rivkin E, Tres LL, Yoder BK, Haycraft CJ, Bornens M & Rios RM. 2011. GMAP210 and IFT88 are present in the spermatid golgi apparatus and participate in the development of the acrosome-acroplaxome complex, head-tail coupling apparatus and tail. *Developmental Dynamics : An Official Publication of the American Association of Anatomists* 240 (3), 723-736.

Kierszenbaum AL & Tres LL. 2004. The acrosome-acroplaxome-manchette complex and the shaping of the spermatid head. *Archives of Histology and Cytology* 67 (4), 271-284.

Kierszenbaum AL, Tres LL, Rivkin E, Kang-Decker N & van Deursen JM. 2004. The acroplaxome is the docking site of Golgi-derived myosin Va/Rab27a/b- containing proacrosomal vesicles in wild-type and Hrb mutant mouse spermatids. *Biology of Reproduction* 70 (5), 1400-1410.

Komada M, McLean DJ, Griswold MD, Russell LD & Soriano P. 2000. E-MAP-115, encoding a microtubule-associated protein, is a retinoic acid-inducible gene required for spermatogenesis. *Genes & Development* 14 (11), 1332-1342.

Korhonen HM, Meikar O, Yadav RP, Papaioannou MD, Romero Y, Da Ros M, Herrera PL, Toppari J, Nef S & Kotaja N. 2011. Dicer is required for haploid male germ cell differentiation in mice. *PloS One* 6 (9), e24821.

Kotaja N, Kimmins S, Brancorsini S, Hentsch D, Vonesch JL, Davidson I, Parvinen M & Sassone-Corsi P. 2004. Preparation, isolation and characterization of stage-specific spermatogenic cells for cellular and molecular analysis. *Nature Methods* 1 (3), 249-254.

Kwitny S, Klaus AV & Hunnicutt GR. 2010. The annulus of the mouse sperm tail is required to establish a membrane diffusion barrier that is engaged during the late steps of spermiogenesis. *Biology of Reproduction* 82 (4), 669-678.

Lehman JM, Michaud EJ, Schoeb TR, Aydin-Son Y, Miller M & Yoder BK. 2008. The Oak Ridge Polycystic Kidney mouse: modeling ciliopathies of mice and men. *Developmental Dynamics : An Official Publication of the American Association of Anatomists* 237 (8), 1960-1971.

Lehti MS, Kotaja N & Sironen A. 2013. KIF3A is essential for sperm tail formation and manchette function. *Molecular and Cellular Endocrinology* 377 (1-2), 44-55.

Liu Y, DeBoer K, de Kretser DM, O'Donnell L, O'Connor AE, Merriner DJ, Okuda H, Whittle B, Jans DA, Efthymiadis A, McLachlan RI, Ormandy CJ, Goodnow CC, Jamsai D & O'Bryan MK. 2015. LRGUK-1 Is Required for Basal Body and Manchette Function during Spermatogenesis and Male Fertility. *PLoS Genetics* 11 (3), e1005090.

Manandhar G, Simerly C, Salisbury JL & Schatten G. 1999. Centriole and centrin degeneration during mouse spermiogenesis. *Cell Motility and the Cytoskeleton* 43 (2), 137-144.

Manandhar G, Sutovsky P, Joshi HC, Stearns T & Schatten G. 1998. Centrosome reduction during mouse spermiogenesis. *Developmental Biology* 203 (2), 424-434.

Meistrich ML, Trostle-Weige PK & Russell LD. 1990. Abnormal manchette development in spermatids of azh/azh mutant mice. *The American Journal of Anatomy* 188 (1), 74-86.

Moore K & Thatcher WW. 2006. Major Advances Associated with Reproduction in Dairy Cattle. *Journal of Dairy Science* 89 (4), 1254-1266.

NCBI. 2016. *National Center for Biotechnology Information. <http://www.ncbi.nlm.nih.gov/ > [Accessed 14.2.2016]*

NICE. 2013. Fertility: Assessment and Treatment for People with Fertility Problems. National Collaborating Centre for Women's and Children's Health <https://www.nice.org.uk/guidance/CG156> [Accessed 2.2.2015]

O'Donnell L, Nicholls PK, O'Bryan MK, McLachlan RI & Stanton PG. 2011. Spermiation: The process of sperm release. *Spermatogenesis* 1 (1), 14-35.

O'Donnell L & O'Bryan MK. 2014. Microtubules and spermatogenesis. *Seminars in Cell & Developmental Biology* 30, 45-54.

Ostrowski LE, Andrews K, Potdar P, Matsuura H, Jetten A & Nettesheim P. 1999. Cloning and characterization of KPL2, a novel gene induced during ciliogenesis of tracheal epithelial cells. *American Journal of Respiratory Cell and Molecular Biology* 20 (4), 675-683.

Otsuka A, Abe T, Watanabe M, Yagisawa H, Takei K & Yamada H. 2009. Dynamin 2 is required for actin assembly in phagocytosis in Sertoli cells. *Biochemical and Biophysical Research Communications* 378 (3), 478-482.

Rosenbaum JL & Witman GB. 2002. Intraflagellar transport. *Nature Reviews.Molecular Cell Biology* 3 (11), 813-825.

Russell LD, Ettlin RA, Hikim APS & Clegg ED. 1993. Histological and histopathological evaluation of the testis. *International Journal of Andrology* 16 (1), 83-83.

Russell LD, Russell JA, MacGregor GR & Meistrich ML. 1991. Linkage of manchette microtubules to the nuclear envelope and observations of the role of the manchette in nuclear shaping during spermiogenesis in rodents. *The American Journal of Anatomy* 192 (2), 97-120.

San Agustin JT, Pazour GJ & Witman GB. 2015. Intraflagellar Transport Is Essential for Mammalian Spermiogenesis but Is Absent in Mature Sperm. *Molecular Biology of the Cell* .

Scholey JM. 1996a. Kinesin-II, a membrane traffic motor in axons, axonemes, and spindles. *The Journal of Cell Biology* 133 (1), 1-4.

Scholey JM. 1996b. Kinesin-II, a membrane traffic motor in axons, axonemes, and spindles. *The Journal of Cell Biology* 133 (1), 1-4.

Sheldon IM & Dobson H. 2003. Reproductive challenges facing the cattle industry at the beginning of the 21st century. *Reproduction (Cambridge, England) Supplement* 61, 1-13.

Sipe CW & Lu X. 2011. Kif3a regulates planar polarization of auditory hair cells through both ciliary and non-ciliary mechanisms. *Development (Cambridge, England)* 138 (16), 3441-3449.

Sironen A, Thomsen B, Andersson M, Ahola V & Vilkki J. 2006. An intronic insertion in KPL2 results in aberrant splicing and causes the immotile short-tail sperm defect in the pig. *Proceedings of the National Academy of Sciences of the United States of America* 103 (13), 5006-5011.

Sironen A, Vilkki J, Bendixen C & Thomsen B. 2007. Infertile Finnish Yorkshire boars carry a full-length LINE-1 retrotransposon within the KPL2 gene. *Molecular Genetics and Genomics : MGG* 278 (4), 385-391.

Sironen A, Hansen J, Thomsen B, Andersson M, Vilkki J, Toppari J & Kotaja N. 2010. Expression of SPEF2 During Mouse Spermatogenesis and Identification of IFT20 as an Interacting Protein. *Biology of Reproduction* 82 (3), 580-590.

Sironen A, Kotaja N, Mulhern H, Wyatt TA, Sisson JH, Pavlik JA, Miiluniemi M, Fleming MD & Lee L. 2011. Loss of SPEF2 Function in Mice Results in Spermatogenesis Defects and Primary Ciliary Dyskinesia. *Biology of Reproduction* 85 (4), 690-701.

Sugimoto R, Nabeshima Y & Yoshida S. 2012. Retinoic acid metabolism links the periodical differentiation of germ cells with the cycle of Sertoli cells in mouse seminiferous epithelium. *Mechanisms of Development* 128 (11-12), 610-624.

Toshimori K & Ito C. 2003. Formation and organization of the mammalian sperm head. *Archives of Histology and Cytology* 66 (5), 383-396.

Turner RM. 2003. Tales from the tail: what do we really know about sperm motility? *Journal of Andrology* 24 (6), 790-803.

Vogl AW, Pfeiffer DC & Redenbach DM. 1991. Ectoplasmic ("junctional") specializations in mammalian Sertoli cells: influence on spermatogenic cells. *Annals of the New York Academy of Sciences* 637, 175-202.

Xiao X, Mruk DD, Wong CK & Cheng CY. 2014. Germ cell transport across the seminiferous epithelium during spermatogenesis. *Physiology (Bethesda, Md.)* 29 (4), 286-298.

Yanagimachi R. 2011. Mammalian sperm acrosome reaction: where does it begin before fertilization? *Biology of Reproduction* 85 (1), 4-5.

Yoshida S. 2012. Elucidating the identity and behavior of spermatogenic stem cells in the mouse testis. *Reproduction (Cambridge, England)* 144 (3), 293-302.

Yoshida S. 2008. Spermatogenic stem cell system in the mouse testis. *Cold Spring Harbor Symposia on Quantitative Biology* 73, 25-32.